Sources and Enrichment Mechanisms of Rare Earth Element in the Mosuoying Granites, Sichuan Province, Southwest China

Xuepeng Xiao , Guoxin Li * , Shuyi Dong , Lijun Qian , Lihua Ou

Posted Date: 16 December 2024

doi: 10.20944/preprints202412.1227.v1

Keywords: Mosuoying A-type granite; Ion-adsorption; REE sources; Magmatic-hydrothermal evolution; extensional setting; Southwest China

 doi:10.20944/preprints202412.1227.v1

Article

Sources and Enrichment Mechanisms of Rare Earth Element in the Mosuoying Granites, Sichuan Province, Southwest China

Xuepeng Xiao [1], Guoxin Li [2,*], Shuyi Dong [1], Lijun Qian [2], Lihua Ou [2]

[1] College of Earth and Planetary Sciences, Chengdu University of Technology, Chengdu 610059, China; xiaoxuepeng99@outlook.com (X.X.); dongshuyi@cdut.cn (S.D.)
[2] Department of Civil and Hydraulic Engineering, Xichang University, Xichang 615000, China; qlj0321@xcc.edu.cn (L.Q); olh886@xcc.edu.cn (L.O.)
* Correspondence: xcc20220323@xcc.edu.cn

Abstract: Ion-adsorption type rare earth elements (iREE) deposits, a primary source of global heavy REE (HREE) ores，have attracted wide attention worldwide due to their concentrated distributions and irreplaceable role in the field of cutting-edge technologies. In recent years, iREE mineralization have been reported in the overlying weathering crust of the Mosuoying granites within the Dechang counties, Sichuan Province, Southwest China, suggesting great potential for the formation of iREE deposits. The Mosuoying granites, acting as the primary carrier of REE pre-enrichment, govern the contents and distribution patterns of REEs in their overlying weathering crust. Therefore, investigating the sources and enrichment mechanisms of REEs in the parent rocks will provide a critical theoretical basis for the scientific exploitation and utilization of iREE deposits. In this study, we investigated the migration and enrichment of REEs in the Mosuoying granites using petrography, geochronology, geochemical and Sr-Nd-Hf isotopic data. The results reveal that the REE enrichment in the Mosuoying granites might be associated with both the melting of crustal felsic rocks and the magmatic-hydrothermal evolution. On the one hand, the granites exhibit different REE patterns. Compared to the light REE (LREE)-rich granites, the HREE-rich granites feature higher SiO_2 contents, higher differentiation index (DI), lower Nb/Ta and Zr/Hf ratios, and more significant negative Eu anomalies, indicating that the crystal fractionation of magmas governed the differentiation of REEs. Furthermore, the hydrothermal fluids further promoted the formation of the HREE-rich granites. On the other hand, the geochemical characteristics suggest that they are A-type granites. Regarding the isotopic characteristics, the Mosuoying granites exhibit negative whole-rock $\varepsilon Nd(t)$ and zircon $\varepsilon Hf(t)$ values, suggesting an evolved crustal source. Therefore, we suggest that the high REE contents in the Mosuoying A-type granites might originate from the partial melting of felsic rocks in a shallow crustal source under high-temperature and low-pressure conditions. Specifically, the high-temperature A-type granitic magmas caused the partial melting of the felsic crustal materials to release REEs; Concurrently, these magmas enhanced the solubility of REEs in melt during magmatic evolution, inhibiting the separation of REE-bearing minerals from the melts. These increased the REE contents of the granites. The high-temperature heat source might be associated with the process where the asthenospheric mantle experienced upwelling along slab window and heated continental crust in the Neoproterozoic extensional setting.

Keywords: Mosuoying A-type granite; Ion-adsorption; REE sources; Magmatic-hydrothermal evolution; extensional setting; Southwest China

1. Introduction

Rare earth elements (REEs) consist of lanthanide elements (La-Lu), yttrium (Y), and scandium (Sc), totaling 17 elements. Because of their unique physical, chemical, magnetic, and optoelectronic properties, REEs are extensively applied in various fields like national defense and aerospace, electronic information, industrial catalysis, medical science, clean energy, electric vehicles, and agronomy [1,2]. Therefore, REEs are known as the "vitamins of modern industry". In recent years, with the continuous advancement in high-tech industries, combined with the uneven REE distribution, the demand for REE ores has steadily increased in various countries [3]. Particularly, heavy rare earth elements (HREEs, i.e., Gd-Lu and Y) have attracted significant attention due to their extremely low contents in the crust and irreplaceable role in the field of cutting-edge technologies [4]. HREEs originate primarily from the iREE deposits in southern China, which provide more than 90% of the world's HREEs [5]. Although iREE deposits occur in weathering profiles in

 doi:10.20944/preprints202412.1227.v1

supergene environments, their formation tends to be governed by the underlying parent rocks. As a significant carrier for the pre-enrichment of REEs, parent rocks typically display REE patterns similar to the overlying weathering crust [6,7]. This inheritance might be the primary cause of various iREE deposits. Therefore, it is necessary to investigate the sources and enrichment mechanisms of REEs in parent rocks. Previous studies have shown that the REE enrichment in the parent rocks might be associated with the melting of rocks in magma sources, which is frequently closely linked with the regional extension against the background of the subduction of oceanic slab [8–10]. Generally, regional extension contributes to the formation of highly differentiated granites, and highly differentiated granitic magmas may facilitate the HREE enrichment in these granites [11]. The large-scale Mesozoic regional extension in South China may account for the formation of ion-adsorption type HREE deposits (iHREE deposits) [10,12,13]. Additionally, external hydrothermal fluids generated by slab subduction could metasomatize the ore-forming parental rocks, facilitating the migration and enrichment of REEs (especially HREEs) in the parent rocks [14,15]. Some researchers held that the REE enrichment in the parent rocks is connected to the magmatic-hydrothermal evolution. The early-stage crystal fractionation of magmas and the late-stage metasomatism of hydrothermal fluids are critical factors controlling the enrichment and distribution patterns of REEs in the parent rocks [7,16,17].

Previous studies on the iREE deposits focus primarily on Mesozoic granitic rocks in South China. However, there is a lack of relevant reports on other regions. In recent years, iREE deposits have been found in Kuanyu Township, Dechang County, Sichuan Province [18,19]. Relevant studies have indicated that this area displays the REE mineralization of the LREE-HREE paragenetic type, and medium-scale iREE mineral resources, suggesting great metallogenic potential [20]. Despite extensive previous studies on the origin of granitic rocks in the study area [21–23], several scientific issues are yet to be addressed: (1) how did the high REE contents in the Mosuoying granites originate? (2) how did the REEs in the parent rocks migrate and get enriched? and (3) why does HREE mineralization occur in the study area? In this paper, we study the petrography, geochronology, geochemical and Sr-Nd-Hf isotopic data of the Mosuoying granites, which aims to solve the following problems: 1) Investigate the the mineralization mechanism of the Mosuoying granites and their implications for the type of ion-adsorbed REE deposits; 2) reveal the sources and enrichment processes of REEs for the Mosuoying granites.

2. Geological Background and Petrology

The study area, located within Dechang-Miyi counties of Sichuan Province, the geotectonic location resides in the middle section of the Kangdian Axis — a second-order tectonic unit along the western margin of the Yangtze Block [24]. The division principle of tectonic units in the Block (Chengdu Geological Survey Center of China Geological Survey, 2012) indicates that the study area is primarily located within the Kangdian basement fault-uplift zone (Class Ⅳ), Kangdian foreland thrust belt (Class Ⅲ), Upper Yangtze ancient continental block (Class Ⅱ), Yangtze craton (Class I) , situated on the Anninghe fault zone in the middle section of the western Sichuan-central Yunnan paleocontinent [25]. The study area experienced intense magmatic activity primarily during the Jinningian and Chengjiangian. Plutons in the study area are dominated by intrusions. They are controlled by deep-seated faults like Mopanshan and Anninghe, extending in the nearly NS direction as batholiths, stocks, and apophyses (Figure 1).

 doi:10.20944/preprints202412.1227.v1

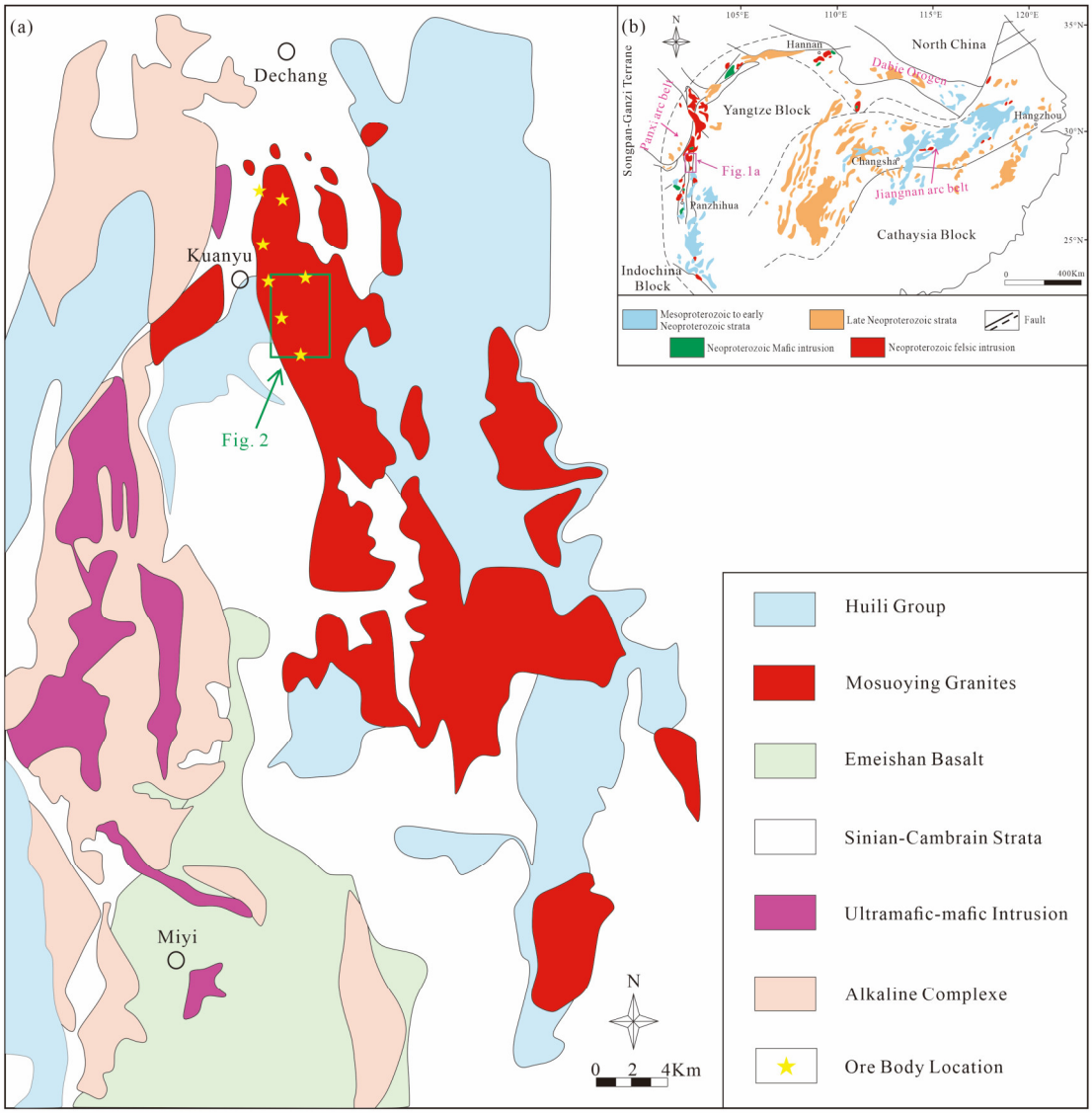

Figure 1. Geological maps showing the distribution of the Mosuoying granites (a: modified after [26]) and the location of the study area in the Yangtze Block, South China (b: modified after [22]).

The Mosuoying granitic pluton is identified as the ore-forming parent rocks in the study area. This pluton exhibits an oblate distribution pattern in the NS direction along the Dechang-Miyi area, spanning approximately 35 km from north to south and 10 km from east to west and covering an exposed area of about 311 km^2 [21,27]. The Mosuoying granitic pluton is composed primarily of intermediate-acidic rocks, followed by mafic rocks. It is a large composite pluton consisting of five rock units: Maoping, Yonglang, Kelang, Ranfanggou, and Huamashan from old to young. These rock units are primarily distributed on the east side of the Cida River, with the Kelang unit being the most developed. The metallogenic area, principally located in the north of the Mosuoying granitic pluton, manifests significant lithology and lithofacies zoning, consisting primarily of light gray porphyritic medium to coarse-grained biotite monzogranites, followed by light gray porphyritic medium to fine-grained (two-mica) monzogranites and light yellowish gray fine-grained granodiorites (Figure 2). The lithofacies zones transition gradually from the central to the marginal facies, with mineral grain sizes and dark minerals gradually decreasing and mineral content progressively increasing [20,21].

 doi:10.20944/preprints202412.1227.v1

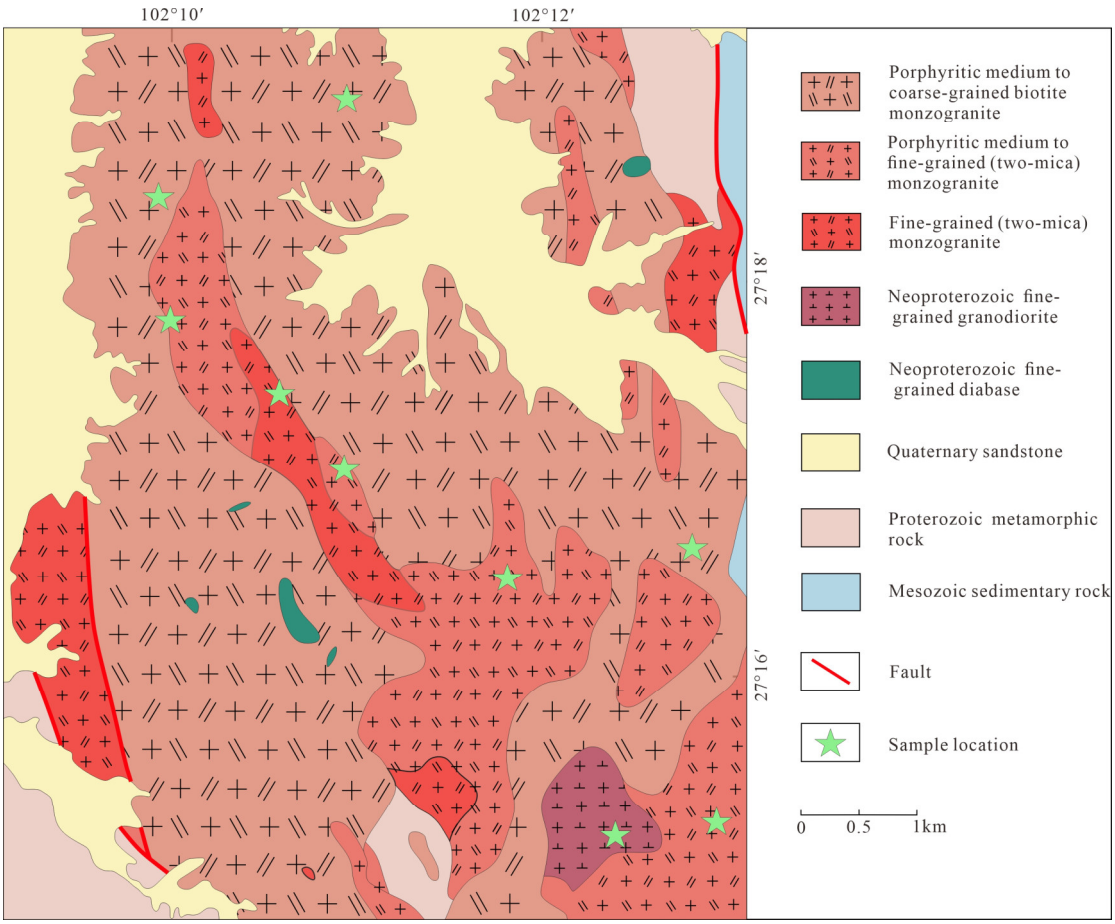

Figure 2. Simplified geological map of Mosuoying granites in the Dechang area, Southwest China.

The light gray porphyritic medium to coarse-grained biotite monzogranites (KY-05, Figure 3a) are composed primarily of plagioclase (35%–40%), K-feldspar (30%–35%), quartz (20%–25%), and biotite (± 5%), with minor accessory minerals such as apatite, zircon, and REE minerals (Figure 3c). Among them, the plagioclase exhibits subhedral tabular textures and significant polysynthetic twinning, with sericitization observed on the surfaces of some plagioclase grains. The K-feldspar displays hypidiomorphic tabular textures and local graphic intergrowth with quartz grains. The quartz occurs as xenomorphic granular crystals filling the cracks between other minerals. The biotite is subhedral lamellar in shape, partially metasomatized by chlorite and accessory minerals. In contrast, the light grayish-white fine-grained (two-mica) monzogranites (KY-08, Figure 3b) consist of plagioclase (35%–40%), K-feldspar (40%–45%), quartz (20%–25%), biotite, muscovite (± 5%), and trace quantities of accessory minerals, with average grain sizes ranging from 0.5 to 2 mm (Figure 3d). Among them, both the plagioclase and potassium feldspar exhibit hypidiomorphic tabular textures, characterized by typical polysynthetic twinning and crossed twinning, respectively. Some plagioclase grains manifest sericitization and are metasomatized by calcite and muscovite (Figure 3e). The biotite is filled between other minerals, showing partial chlorite alteration (Figure 3f).

 doi:10.20944/preprints202412.1227.v1

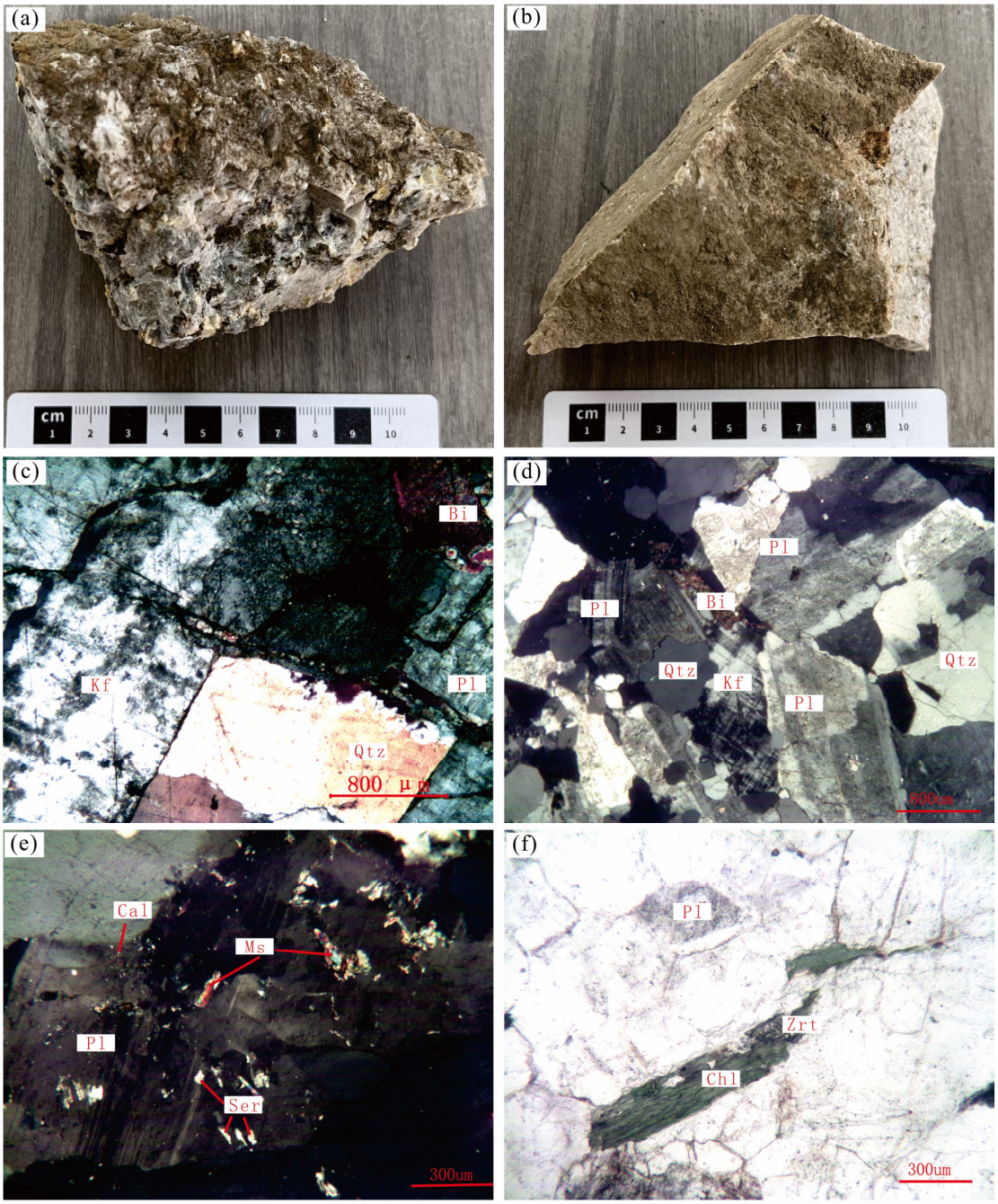

Figure 3. Hand specimen and representative microscope photographs of the Mosuoying granites. Pl–plagioclase; Kfs–K-feldspar; Qtz–quartz; Bi-biotite; Ms–muscovite; Ser–Sericite; Chl–chlorite; Zrt–zircon; Cal–calcite.

3. Analytical Methods

In this study, zircon geochronology, major and trace element analyses, whole-rock Sr-Nd isotopic analyses, and in situ zircon Hf isotopic analyses were completed at the Langfang Shangyi Geological Exploration Technical Services Co., Ltd (LSGETS). Back-scattered electron (BSE) images of REE-bearing minerals were obtained at the Institute of Multipurpose Utilization of Mineral Resources, Chinese Academy of Geological Sciences.

3.1. REE-Bearing Minerals

The BSE images of REE-bearing minerals in the rock samples were obtained using an FEI Quanta 250 scanning electron microscope (SEM) equipped with an energy-dispersive X-ray spectrometer (EDS). Tests were completed at a voltage of 20 kV and a current of 10 nA.

3.2. Zircon U-Pb Dating

 doi:10.20944/preprints202412.1227.v1

Zircon grains from the samples were separated using heavy liquid and magnetic separation techniques. Representative zircon grains selected under a binocular microscope were placed in epoxy resin disks for polishing and carbon coating. Afterward, their cathodoluminescence (CL) and BSE images were obtained using a MIRA3 SEM. Then, zircon grains with clear internal oscillatory zoning and without surface cracks and inclusions were selected for U-Pb isotopic analyses. Zircon U-Pb dating was conducted using an iCAPQ inductively coupled plasma mass spectrometer (ICP-MS) equipped with a 193 nm GeoLasPro laser ablation system. Helium was employed as a carrier gas, mixed with argon (auxiliary gas) via a T-connector before laser ablation sampling. Harvard zircon 91500 was used as an external reference for U-Pb dating, with recommended $^{207}Pb/^{235}U$ and $^{206}Pb/^{238}U$ isotopic ages of 1063.35 Ma and 1062.45 Ma, respectively. The Plešovice zircon was also used as a certified reference material with recommended $^{206}Pb/^{238}U$ isotopic ages of 337.13 ± 0.37 Ma [28]. The isotopic ratios were calculated using the Excel-based software ICPMSDataCal. The plotting of concordia diagrams and the calculation of weighted mean ages were performed using Isoplot 3.0 [29].

3.3. Whole-Rock Major and Trace Element Analyses

The fresh parts of the whole-rock samples were ground into about 200 mesh fractions using an agate ball mill. For major element analyses, rock powders (0.6 g) were blended evenly with a mixed solvent of $Li_2B_4O_7$ (4.5 g), $LiBO_2$ (1.0 g), and LiBr (0.5 g). Then, melt tablets were prepared for X-ray fluorescence spectrometry (XRFS) analysis using an Axios Max Minerals spectrometer. Trace elements were analyzed using an iCAP Qc ICP-MS. Samples powders were digested using a mixture of HNO_3 (0.5 ml) and HF (1 ml) in Teflon bombs at a temperature of 185℃ ±5℃. The analytical precision and accuracy for the major and trace elements were all better than 5%.

3.4. Whole-Rock Sr-Nd Isotopic Analyses

Whole-rock Sr-Nd isotopic compositions were conducted at the LSGETS using a Neptune MC-ICP-MS produced by Thermo Fisher Scientific Inc. The Sr and Nd separation in the digestion solution was achieved in three steps. First, Sr was separated from the sample matrix using Sr Spec resin (100–150 μm). Then, REEs were prepared using cation exchange resin (AG502X12). Finally, Nd was separated from REEs using Ln Spec resin. The isotopic fractionation of Sr and Nd was corrected to $^{88}Sr/^{86}Sr = 8.375209$ and $^{146}Nd/^{144}Nd = 0.7219$, respectively.

3.5. Zircon Hf isotopic Analyses

In-situ zircon Hf isotopic data were obtained using a Nu Plasma II MC-ICP-MS manufactured by Nu Instruments (Wrexham, Wales, UK) and a RESOlution LR S-155 excimer ArF laser ablation system at the LSGETS. During sample ablation for 40 s, the isotopic analysis was conducted in a single-point mode, with a laser spot size of 50 μm, a repetition frequency of 9 Hz, and an energy density of 4.5 J/cm². Concurrently, zircon standards 91,500, GJ-1, and Plešovice were analyzed to ensure accurate analytical data. The Hf isotopic compositions of 91,500, GJ-1, and Plešovice were determined at 0.282307 ± 0.000020 (2σ, n = 16), 0.282010 ± 0.000016 (2σ, n = 12), and 0.282479 ± 0.000014 (2σ, n = 23), respectively, aligning with the reference values within the error range.

4. Results

4.1. Characteristics of REE-Bearing Minerals

The Mosuoying granites contain diverse REE-bearing minerals. Among them, LREE-rich granites exhibit REE-bearing minerals such as monazite, titanite, allanite, apatite, thorite, zircon, and bastnasite. In contrast, the HREE-rich granite displays more REE-bearing minerals. Besides the abovementioned minerals, the HREE-rich granites contain many Y-rich REE-bearing minerals like fergusonite, orthorhombic pyroxene-(Y), Y- and Th-rich silicate minerals, and yttrocrasite. The BSE images show that these various REE-bearing minerals have multiple occurrence modes. Among them, the monazite occurs mostly as irregular grains (grain size: below 20 μm), housed in albite and allanite in the form of inclusions (Figure 4a, d). The allanite feature varying internal textures and brightness and light gray and homogeneous grain centers, suggesting primary magmatic allanite. Some allanite exhibits dark gray grain edges, which are suspected to be the accretionary boundary formed by hydrothermal fluid-induced alteration (Figure 4d). The titanite occurs as idiomorphic and rhombic crystals (grain size: 15–20 μm), associated with apatite, zircon, and bastnasite (Figure 4b). The thorite, zircon, apatite, and bastnasite are typically paragenetic as mineral aggregates (Figure 4c, g), with the formation of the thorite and bastnasite likely related to the metasomatic replacement of primary magmatic zircons by hydrothermal fluids. The fergusonite (grain size: 5–20 μm) largely occurs as idiomorphic independent minerals within mica minerals (Figure 4e). The orthorhombic pyroxene-(Y) and Y- and Th-rich silicate minerals, exhibiting tabular or prismatic morphologies, are paragenetic with zircon, siderite, and K-feldspar (Figure 4f). The yttrocrasite displays significant zonal textures (Figure 4h, i), with brighter Yttrocrasite having higher Y contents.

Preprints.org (www.preprints.org) | NOT PEER-REVIEWED | Posted: 16 December 2024 doi:10.20944/preprints202412.1227.v1

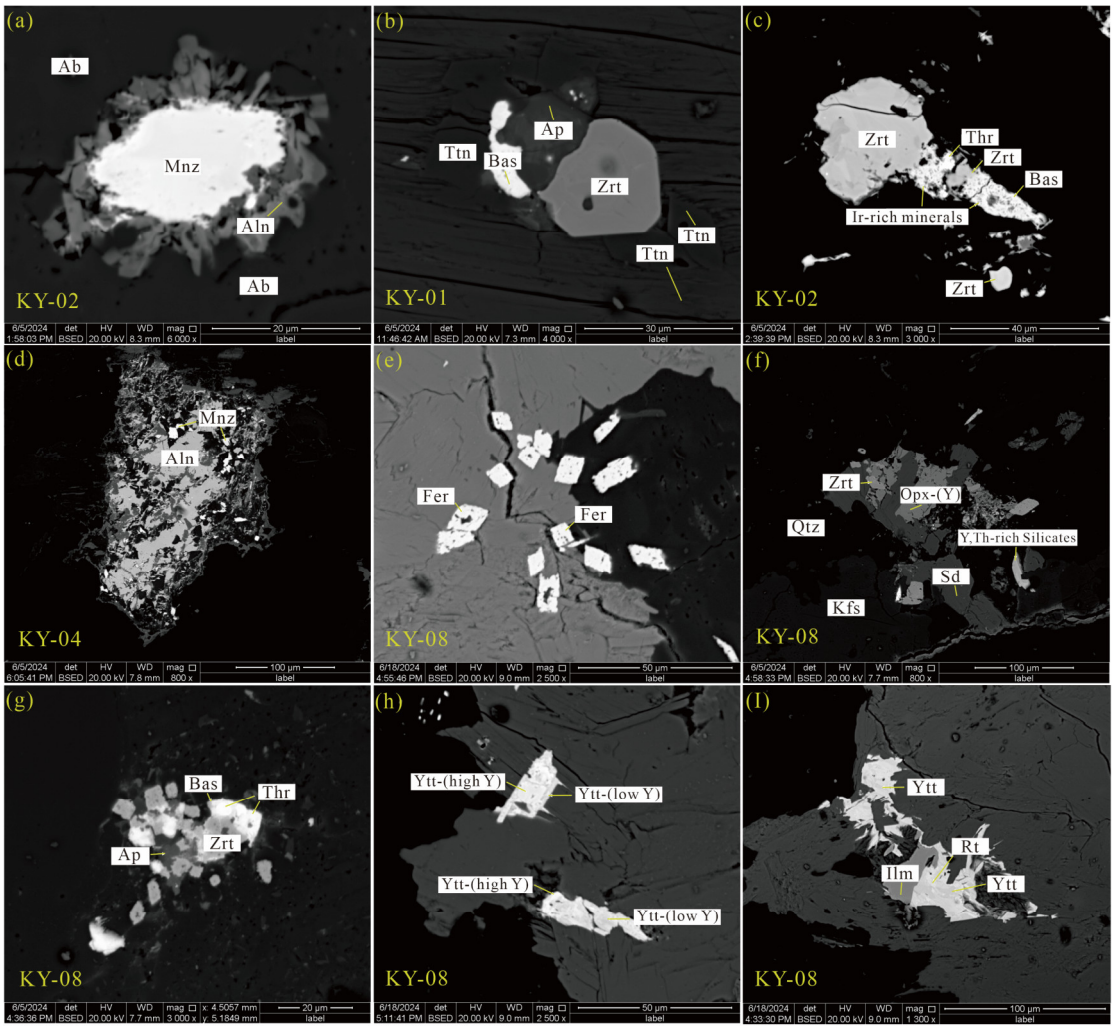

Figure 4. BSE images of REE-bearing minerals in samples from the Mosuoying granites. Mineral abbreviations: Mnz–monazite, Aln–allanite, Ab–Albite, Ttn–titanite, Bas–bastnasite, Zrt–zircon, Ap–apatite, Thr–thorite, Fer–fergusonite, Opx-(Y)–orthorhombic pyroxene-(Y), Sd–siderite, Kfs–K-feldspar, Qtz–quartz, Ytt–yttrocrasite, Rt–rutile, Ilm–ilmenite.

4.2. Zircon U-Pb Dating Results

The LREE-rich granite (KY-05) and HREE-rich granite (KY-08) samples from the Mosuoying granitic pluton were selected for zircon U-Pb dating. Their typical zircon CL images and U-Pb age concordia diagrams are illustrated in Figure 5 and Figure 6, respectively, and their U-Pb analytical data are presented in Table 1.

The zircon grains in the LREE-rich granite sample (KY-05) exhibit high automorphic degrees, mostly occurring as long prismatic idiomorphic-hypidiomorphic crystals. These grains measure from 80 to 220 μm in size, with length/width ratios ranging from 2:1 to 3:1 (Figure 5a). A total of 15 analytical spots were tested in this sample. The results indicate that the zircons in the sample manifested U contents ranging from 132 to 671 ppm and Th contents from 97 to 246 ppm, with Th/U ratios varying between 0.39 and 0.97 (average: 0.62). Most zircons from the sample display high Th and U contents and Th/U ratios (above 0.4) and notable oscillatory zoning, suggesting typical magmatic zircon [30–32]. The U-Pb age concordia diagram indicates that 13 reliable analytical spots in the KY-05 sample exhibit $^{206}Pb/^{238}U$ ages ranging from 831 ± 8 to 875 ± 7 Ma, with a weighted mean age of 849.7 ± 7.8 Ma (MSWD = 2.6, n = 13, Figure 6a, b), which represents the crystallization age of the LREE-rich granites.

The zircon grains in the HREE-rich granite sample (KY-08) mostly occur as short prismatic hypidiomorphic-idiomorphic crystals, exhibiting relatively complete crystal forms. These grains measure from 46 to 140 μm in size, with length/width ratios varying between 1:1 and 3.5:1. Most of these grains display clear oscillatory zoning on their crystal planes, suggesting typical magmatic zircon (Figure 5b). A total of 20 analytical spots in this sample were tested. The U-Pb age concordia diagram shows that analytical spots 01, 03, 08, 09, and 15 fall below the concordia line, suggesting that the measured ages are less than the actual crystallization ages. This result implies that the U-Pb systems at the five analytical spots experienced late-stage geologic events, leading to the loss of radiogenic Pb in the zircons [33]. For analytical point 12, the measured age was much older than the actual crystallization age of the Mosuoying granitic

 doi:10.20944/preprints202412.1227.v1

pluton, suggesting inherited zircons from surrounding rocks during magmatic emplacement. Analytical point 11 deviates from the U-Pb concordia line and thus cannot represent the crystallization age of the pluton. Except for the above analytical spots, nine reliable analytical spots fall on or near the concordia line, indicating $^{206}Pb/^{238}U$ ages between 816 ± 8 Ma and 848 ± 9 Ma, with a weighted mean age of 833.3 ± 8 Ma (MSWD = 1.9, n=9, Figure 6c, d), which represents the crystallization age of the HREE-rich granites.

In conclusion, the Mosuoying granites were formed at ca. 833-850 Ma, corresponding to the Neoproterozoic.

Table 1. LA-ICP-MS zircon U-pb analytical data of the Mosuoying granites in the study area.

Sample No	Th ppm	U ppm	Th/U	U-Th-Pb isotopic ratio								Age (Ma)							
				$^{207}Pb/^{206}Pb$	1σ	$^{207}Pb/^{235}U$	1σ	$^{206}Pb/^{238}U$	1σ	$^{208}Pb/^{232}Th$	1σ	$^{207}Pb/^{206}Pb$	1σ	$^{207}Pb/^{235}U$	1σ	$^{206}Pb/^{238}U$	1σ	$^{208}Pb/^{232}Th$	1σ
KY-05																			
01	193	296	0.65	0.06626	0.00127	1.28018	0.02483	0.14000	0.00120	0.04314	0.00066	815	39	837	11	845	7	854	13
02	90.2	132	0.68	0.07042	0.00170	1.35085	0.03499	0.13908	0.00161	0.04179	0.00083	943	45	868	15	839	9	828	16
03	166	291	0.57	0.06700	0.00130	1.34231	0.02597	0.14533	0.00124	0.04469	0.00073	839	40	864	11	875	7	884	14
04	246	671	0.37	0.06642	0.00096	1.30827	0.02109	0.14263	0.00141	0.04322	0.00075	820	30	849	9	860	8	855	15
05	104	148	0.70	0.07064	0.00168	1.34409	0.03524	0.13753	0.00163	0.04243	0.00080	946	48	865	15	831	9	840	15
06	141	177	0.79	0.06764	0.00138	1.30692	0.02830	0.14003	0.00159	0.03985	0.00064	857	42	849	12	845	9	790	12
07	126	174	0.72	0.06565	0.00177	1.28525	0.03574	0.14213	0.00187	0.04327	0.00079	794	56	839	16	857	11	856	15
08	207	312	0.67	0.06636	0.00134	1.29893	0.02785	0.14171	0.00149	0.04262	0.00073	817	43	845	12	854	8	844	14
09	183	248	0.74	0.06552	0.00149	1.29019	0.02838	0.14323	0.00158	0.04216	0.00068	791	48	841	13	863	9	835	13
10	131	218	0.60	0.06518	0.00144	1.37827	0.03497	0.15307	0.00205	0.04764	0.00097	789	47	880	15	918	11	941	19
11	87.1	225	0.39	0.06549	0.00146	1.27094	0.02931	0.14051	0.00124	0.04183	0.00079	791	46	833	13	848	7	828	15
12	109	283	0.39	0.06634	0.00119	1.25833	0.02381	0.13755	0.00144	0.04284	0.00070	817	32	827	11	831	8	848	13
13	161	347	0.46	0.06524	0.00118	1.27030	0.02445	0.14095	0.00121	0.04498	0.00077	783	39	833	11	850	7	889	15
14	137	158	0.87	0.06707	0.00165	1.28405	0.03330	0.13882	0.00165	0.04235	0.00080	839	56	839	15	838	9	838	15
15	129	289	0.45	0.06736	0.00157	1.42050	0.04111	0.15237	0.00233	0.04936	0.00109	850	49	898	17	914	13	974	21
KY-08																			
01	2454	6351	0.39	0.06523	0.00113	0.59374	0.01087	0.06584	0.00081	0.01900	0.00051	783	35	473	7	411	5	380	10
02	361	308	1.17	0.07032	0.00157	1.32532	0.02936	0.13635	0.00129	0.04164	0.00067	939	42	857	13	824	7	825	13
03	366	295	1.24	0.05261	0.00158	0.40154	0.01272	0.05510	0.00063	0.01712	0.00028	322	73	343	9	346	4	343	6
04	492	1159	0.42	0.07043	0.00104	1.32926	0.02021	0.13653	0.00123	0.04433	0.00059	943	31	859	9	825	7	877	11
05	483	1703	0.28	0.06621	0.00098	1.21120	0.01926	0.13216	0.00117	0.03176	0.00070	813	30	806	9	800	7	632	14
06	199	305	0.65	0.06718	0.00137	1.23369	0.02479	0.13302	0.00138	0.04082	0.00063	843	-158	816	11	805	8	809	12
07	186	265	0.70	0.06677	0.00131	1.24488	0.02478	0.13499	0.00144	0.04205	0.00062	831	41	821	11	816	8	832	12
08	251	364	0.69	0.05452	0.00156	0.44474	0.01233	0.05913	0.00053	0.01804	0.00032	394	65	374	9	370	3	361	6
09	405	509	0.80	0.06979	0.00174	0.59865	0.01454	0.06242	0.00100	0.02250	0.00035	924	51	476	9	390	6	450	7
10	384	409	0.94	0.07518	0.00151	1.34947	0.02982	0.12953	0.00127	0.04172	0.00078	1073	45	867	13	785	7	826	15

 doi:10.20944/preprints202412.1227.v1

11	527	693	0.76	0.37045	0.00871	3.44825	0.10373	0.06695	0.00088	0.09578	0.00382	3794	36	1515	24	418	5	1849	70
12	239	193	1.24	0.11551	0.00173	5.27910	0.08117	0.33034	0.00283	0.09412	0.00125	1888	27	1865	13	1840	14	1818	23
13	397	562	0.71	0.07451	0.00170	1.43403	0.03242	0.13940	0.00143	0.05016	0.00448	1055	46	903	14	841	8	989	86
14	201	314	0.64	0.06713	0.00115	1.30399	0.02340	0.14062	0.00155	0.04117	0.00059	843	36	847	10	848	9	816	12
15	503	351	1.43	0.12010	0.00660	0.77236	0.04909	0.04544	0.00050	0.01791	0.00065	1958	98	581	28	286	3	359	13
16	190	205	0.92	0.06805	0.00133	1.28945	0.02564	0.13696	0.00115	0.04005	0.00056	870	40	841	11	827	7	794	11
17	259	372	0.70	0.06707	0.00121	1.28975	0.02325	0.13913	0.00117	0.03931	0.00054	839	-162	841	10	840	7	779	10
18	206	335	0.62	0.06594	0.00126	1.27282	0.02257	0.14004	0.00146	0.04032	0.00059	806	40	834	10	845	8	799	11
19	264	433	0.61	0.07959	0.00215	1.45701	0.03381	0.13339	0.00129	0.04868	0.00122	1187	53	913	14	807	7	961	24
20	275	591	0.47	0.06670	0.00117	1.27296	0.02212	0.13806	0.00128	0.04112	0.00063	828	37	834	10	834	7	814	12

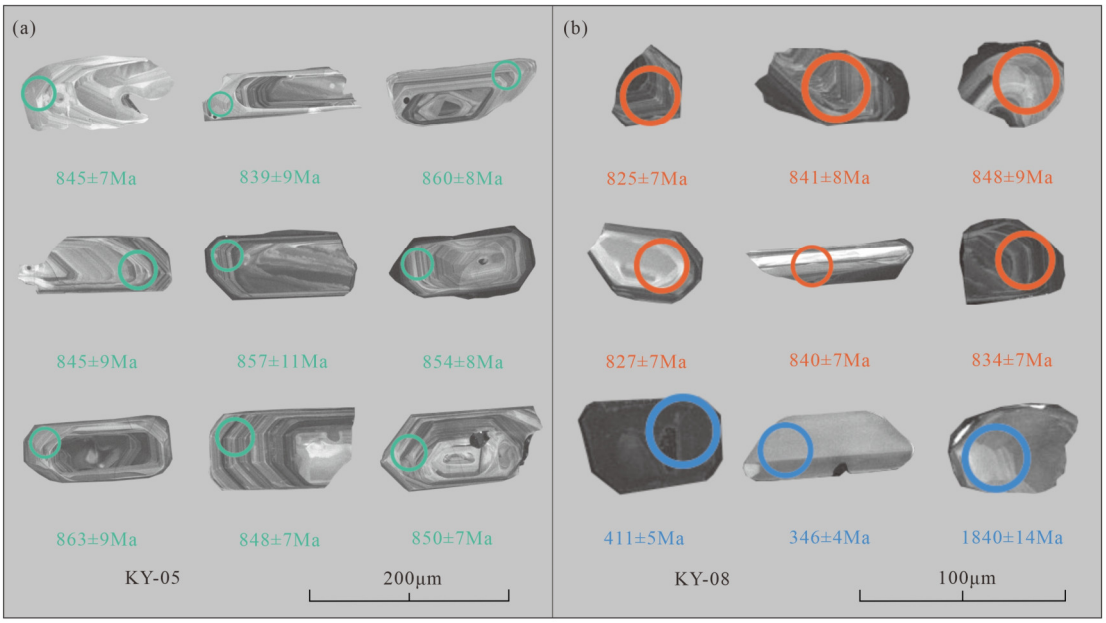

Figure 5. Representative cathodoluminescence (CL) images of zircon grains for the LREE-rich granite (5a) and HREE-rich granite (5b) in the study area.

Preprints.org (www.preprints.org) | NOT PEER-REVIEWED | Posted: 16 December 2024 doi:10.20944/preprints202412.1227.v1

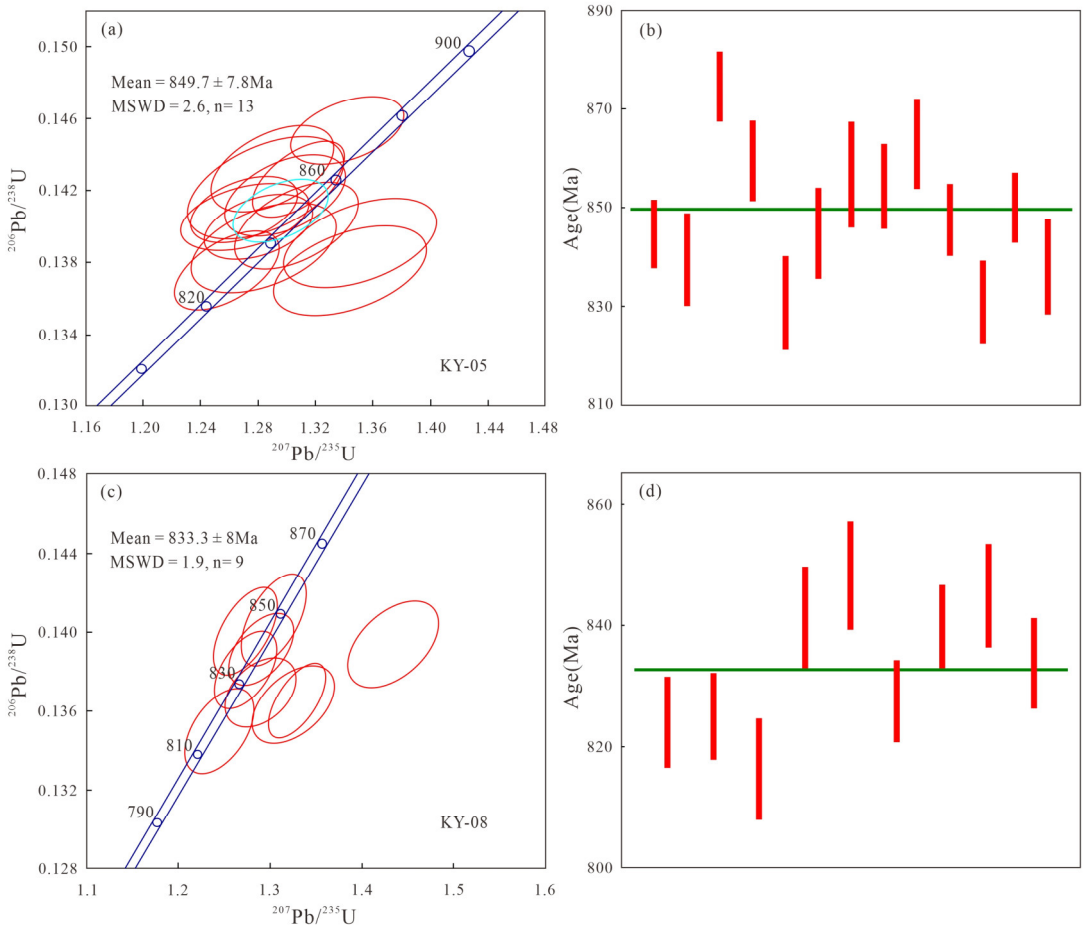

Figure 6. LA-ICP-MS U-Pb zircon concordia diagrams for the LREE-rich granite (6a-b) and HREE-rich granite (6c-d) in the study area.

4.3. Whole-Rock Major- and Trace Element and REE Compositions

The whole-rock major- and trace element and REE compositions of all samples are listed in Table 2. The results indicate that the samples had high contents of SiO_2 (70.55–78.34 wt.%; average: 75.10 wt.%) and $Na_2O + K_2O$ (7.03–8.34 wt.%; average: 7.90 wt.%) and moderate contents of Al_2O_3 (11.35–15.20 wt.%; average: 12.88 wt.%). Furthermore, these samples are depleted in MgO (0.04–0.54 wt.%), CaO (0.33–1.79 wt.%), TiO_2 (0.03–0.33 wt.%), and P_2O_5 (0.01–0.10 wt.%). With an increase in the SiO_2 contents, the Al_2O_3, TiO_2, Fe_2O_3, P_2O_5, MgO, and CaO contents all show a downward trend (Figure 8). The rock samples fall within the subalkalic zone in the $(Na_2O + K_2O)$ *vs.* SiO_2 diagram (Figure 7a), primarily within the high-K calc-alkaline - shoshonitic zone in the SiO_2 *vs.* K_2O diagram (Figure 7b), and all within the alkalic zone in the A.R *vs.* SiO_2 diagram (Figure 7d). The A/NK *vs.* A/CNK diagram shows high A/NK (1.08–1.47) and A/CNK ratios (1.00–1.63) of all these samples, suggesting peraluminous characteristics (Figure 7c). Moreover, the Mosuoying granites have high total REE contents (∑REE = 266.91–553.88 ppm). The chondrite-normalized REE patterns diagram (Figure 9a) shows that all samples except for KY-08 are enriched LREEs (La_N/Yb_N = 3.68–16.07). All the samples display significant negative Eu anomalies (δEu = 0.05–0.41). The primitive-mantle normalized trace element spidergram (Figure 9b) indicates that the samples are enriched in Rb, Th, U, K, and Pb and depleted in Ba, Nb, Ta, Sr, P, and Ti.

Among all samples, sample KY-08 is significantly enriched in HREEs (L/HREE = 0.24). The major-element characteristics reveal that this sample exhibit alkalinity, with higher SiO_2 contents and lower TiO_2, Fe_2O_3, P_2O_5, MgO, and CaO contents than the LREE-rich granites (Figure 8). The trace-element characteristics reveal that this sample have lower Nb/Ta and Zr/Hf ratios. Besides, the REE characteristics indicate that this sample is characterized by significant negative Eu anomalies (δEu = 0.05) and high Y contents (231.21 ppm).

Table 2. Major element (wt.%) and trace element (ppm) compositions of the rock samples from the Mosuoying granites.

Sample	KY-01	KY-02	KY-03	KY-04	KY-05	KY-06	KY-07	KY-08

 doi:10.20944/preprints202412.1227.v1

	LREE-rich granite							HREE-rich granite
SiO_2	73.30	76.98	77.02	73.12	76.73	70.55	74.74	78.34
TiO_2	0.29	0.14	0.11	0.33	0.10	0.33	0.08	0.03
Al_2O_3	13.40	11.35	11.94	13.20	12.27	15.20	13.76	11.90
$Fe_2O_3^T$	2.68	1.83	1.64	2.43	1.52	2.87	1.44	0.47
MnO	0.028	0.014	0.018	0.029	0.018	0.028	0.028	0.006
MgO	0.26	0.12	0.32	0.54	0.09	0.39	0.08	0.04
CaO	1.15	0.46	0.47	1.79	0.52	0.99	0.33	0.42
Na_2O	2.82	2.67	2.52	3.64	2.56	2.63	2.84	3.80
K_2O	5.36	5.67	5.06	3.39	4.96	5.57	5.31	4.39
P_2O_5	0.07	0.02	0.03	0.09	0.02	0.10	0.01	0.01
LOI	0.48	0.63	0.73	1.30	1.06	1.12	1.25	0.46
TOTAL	99.82	99.87	99.86	99.84	99.84	99.78	99.86	99.87
A/CNK	1.07	1.00	1.14	1.02	1.17	1.25	1.25	1.01
A/NK	1.28	1.08	1.08	1.37	1.28	1.47	1.32	1.08
DI	89.48	95.16	93.33	86.29	93.50	87.43	93.55	97.07
SI	2.35	1.17	3.39	5.45	1.02	3.49	0.80	0.50
Li	18.45	8.50	7.80	17.66	10.97	10.47	15.04	2.09
Be	4.00	4.32	3.16	4.06	4.59	3.26	5.57	23.05
Sc	6.50	6.97	7.73	8.62	7.17	7.46	7.54	5.16
V	8.43	4.24	2.42	10.71	3.07	15.09	4.68	3.00
Cr	6.32	3.50	ND	5.80	4.33	9.08	4.90	2.53
Co	2.22	1.08	0.74	2.68	0.65	3.49	0.56	0.82
Ni	0.92	0.66	ND	1.30	1.33	0.37	0.55	0.49
Cu	1.34	1.09	3.88	12.47	2.18	2.44	2.02	2.25
Zn	39.37	25.91	22.20	26.63	26.50	31.66	23.75	7.75
Ga	24.83	24.86	26.6	26.31	25.01	26.32	24.77	21.46
Rb	292.02	298.85	300.00	186.07	378.04	217.67	480.32	292.12
Sr	76.87	24.31	36.40	111.85	21.19	106.29	28.70	25.17
Sn	5.26	5.67	8.72	6.30	8.66	6.37	12.84	4.19
Cs	5.09	3.08	2.10	1.90	4.69	2.04	8.53	1.40
Ba	499.20	54.64	118.00	424.36	121.62	1019.83	155.73	122.79
Tl	1.54	1.38	1.29	0.97	1.70	0.81	2.33	1.33
Pb	24.69	29.63	33.00	13.75	10.47	0.49	11.00	31.07
Th	46.87	47.24	50.00	45.18	57.42	51.87	45.84	32.65
U	5.01	6.74	10.40	7.78	9.58	4.32	9.37	11.99
Nb	12.60	12.53	13.00	16.39	13.30	13.82	19.06	14.43
Ta	1.10	1.32	1.50	1.79	1.69	1.29	3.58	2.26
Zr	153.91	190.08	146.00	183.44	275.80	166.02	237.24	192.80
Hf	6.21	7.72	5.18	7.07	10.59	5.14	9.98	12.47
Zr/Hf	24.79	24.62	28.19	25.95	26.04	32.33	23.78	15.46
Nb/Ta	11.50	9.47	8.67	9.15	7.87	10.68	5.33	6.38
Rb/Sr	3.80	12.29	8.24	1.66	17.84	2.05	16.74	11.60
La	87.42	85.78	53.40	76.23	88.08	69.06	37.39	14.96
Ce	180.36	173.15	124.00	154.05	145.65	169.13	72.86	33.61
Pr	19.30	19.95	14.10	16.91	24.39	17.33	10.28	3.87
Nd	74.02	74.08	51.40	66.21	93.09	61.52	40.87	18.63
Sm	13.77	14.04	11.40	13.61	19.47	11.62	10.38	9.18
Eu	0.91	0.24	0.28	0.85	0.49	1.46	0.30	0.22
Gd	12.08	11.88	9.82	12.89	19.82	10.42	10.12	17.67

Preprints.org (www.preprints.org) | NOT PEER-REVIEWED | Posted: 16 December 2024 doi:10.20944/preprints202412.1227.v1

Tb	1.81	1.90	1.77	2.13	3.32	1.60	1.75	3.90
Dy	9.38	10.43	9.55	11.96	19.22	8.84	10.10	28.99
Ho	1.75	2.01	1.91	2.43	4.06	1.82	2.13	6.84
Er	4.66	5.81	5.58	7.00	11.35	5.08	6.59	21.36
Tm	0.66	0.88	0.92	1.04	1.72	0.76	1.06	3.48
Yb	3.90	5.40	5.92	6.37	10.63	4.72	7.28	21.77
Lu	0.57	0.77	0.86	0.93	1.54	0.66	1.13	3.25
Y	43.55	45.57	49.90	68.25	111.03	50.49	54.66	231.21
∑REE	454.13	451.88	340.81	440.84	553.88	414.51	266.91	418.93
∑LREE	375.77	367.23	254.58	327.85	375.77	367.23	80.46	80.46
∑HREE	78.36	84.64	86.23	112.99	182.70	84.38	94.82	338.47
L/HREE	4.80	4.34	2.95	2.90	2.03	3.91	1.81	0.24
δEu	0.22	0.06	0.08	0.20	0.08	0.41	0.09	0.05
δCe	1.08	1.03	1.11	1.05	0.77	1.20	0.91	1.08
$(La/Yb)_N$	16.07	11.40	6.47	8.58	5.94	10.50	3.68	0.49

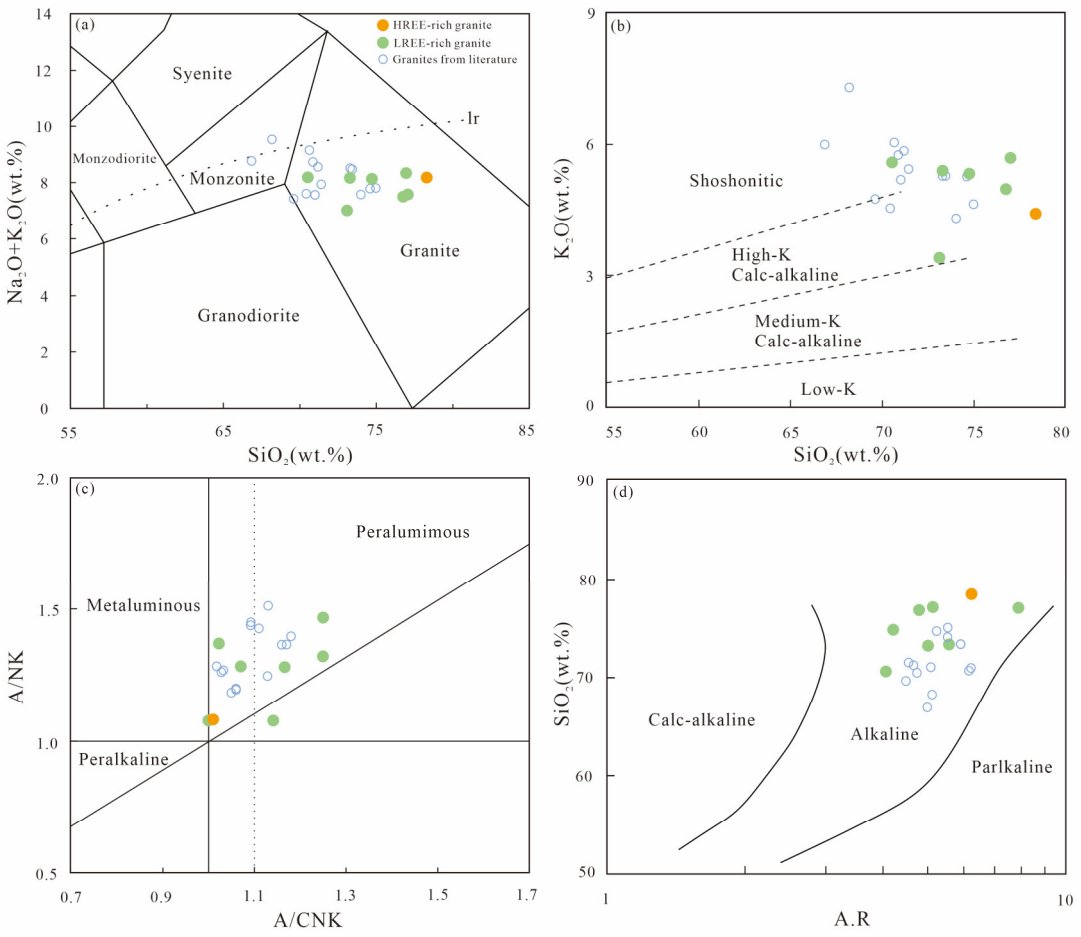

Figure 7. (a) ($Na_2O + K_2O$) vs. SiO_2 diagram [34]; (b) K_2O vs. SiO_2 diagram [35]; (c) A/NK vs. A/CNK diagram [36](Maniar and Piccoli, 1989); (d) SiO_2 vs. A.R diagram [37]; The data for granites from literature are from [21,23,26].

Preprints.org (www.preprints.org) | NOT PEER-REVIEWED | Posted: 16 December 2024 doi:10.20944/preprints202412.1227.v1

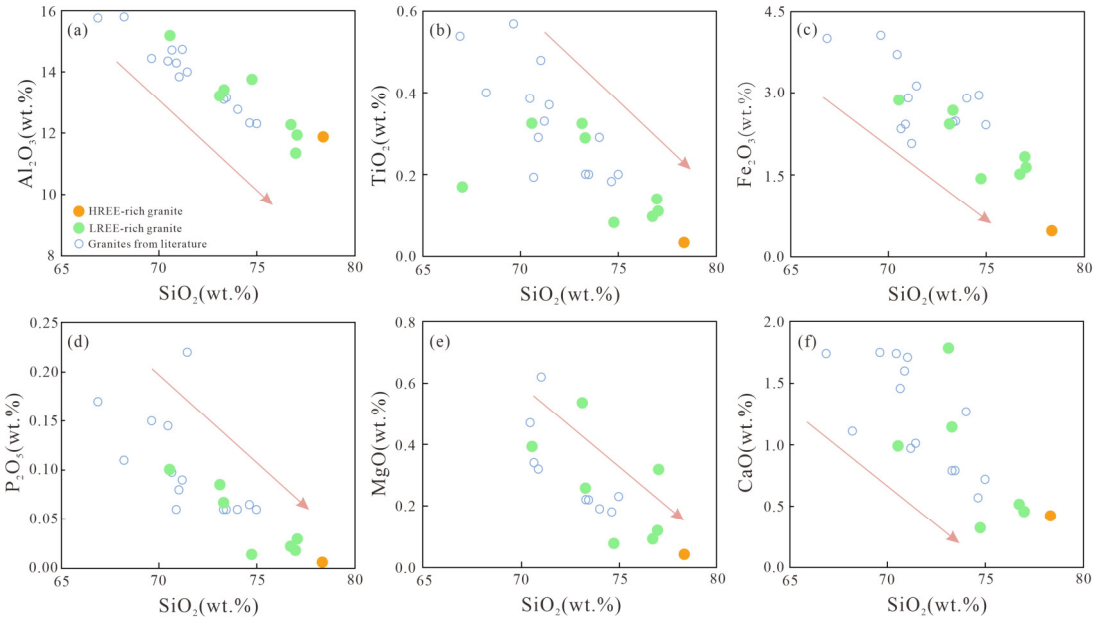

Figure 8. Harker variation diagrams for major-element oxides of samples from the Mosuoying granites. The data sources identical to Figure 7.

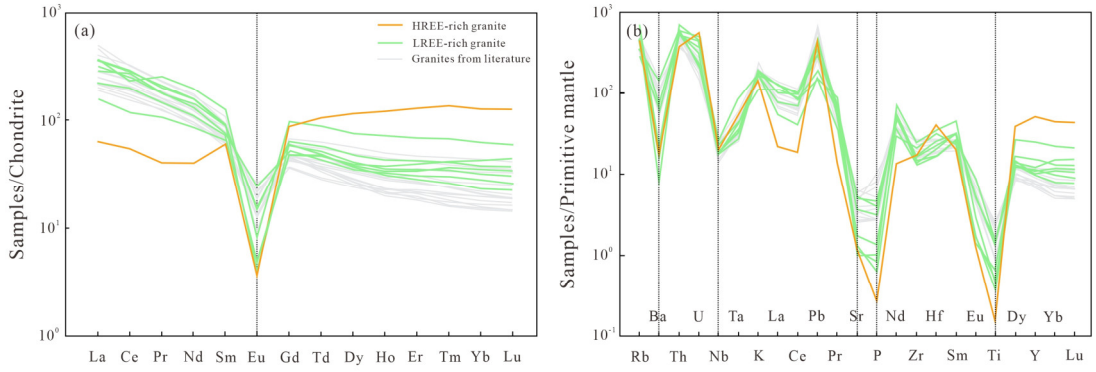

Figure 9. (a) Chondrite-normalized REE patterns and (b) primitive mantle-normalized trace element spidergram for samples from the Mosuoying granites. Normalized values of the primitive mantle and chondrite are from [38]. The data sources identical to Figure 7.

4.4. Whole-Rock Sr-Nd Isotopic Results

In this study, three typical granite samples, i.e., KY-01, KY-05, and KY-08, from the Mosuoying granites were selected for whole-rock Sr-Nd isotopic analysis (Table 3 and Figure 10). These samples exhibited initial $^{87}Sr/^{86}Sr$ ratios $(^{87}Sr/^{86}Sr)_i$ varying from 0.700121 to 0.729158. Their εNd(t) values ranged from -5.8 to -4.3, indicating Nd enrichment. Additionally, these samples showed ancient two-stage Nd model ages (Nd-T_{2DM}) ranging between 1839 and 1966 Ma.

4.5. Zircon Hf Isotopic Results

In-situ Lu-Hf isotopic analysis was conducted on zircon grains from representative granite samples KY-05 and KY-08 (Table 4 and Figure 10). Fifteen analytical spots in sample KY-05 yield initial $^{176}Hf/^{177}Hf$ ratios $(^{176}Hf/^{177}Hf)_i$ ranging from 0.282132 to 0.282202. Zircon grains from this sample display εNd(t) values ranging from -4.7 to -2.2, corresponding to Hf-T_{2DM} from 1835 to 1989 Ma. Zircons from sample KY-08 manifest initial $^{176}Hf/^{177}Hf$ ratios varying from 0.282113 to 0.282233. All analytical spots of this sample reveal negative εNd(t) values ranging from -5.1 to -0.9 and relatively ancient Hf-T_{2DM} from 1761 to 2026 Ma.

Table 3. Whole rock Sr-Nd isotopic data for the Mosuoying granites in the study area.

Sample	$^{87}Rb/^{86}Sr$	$^{87}Sr/^{86}Sr$	±2σ	$(^{87}Sr/^{86}Sr)i$	$^{147}Sm/^{144}Nd$	$^{143}Nd/^{144}Nd$	±2σ	$(^{143}Nd/^{144}Nd)_i$	εNd(t)	T_{2DM}

 doi:10.20944/preprints202412.1227.v1

KY-01	10.99	0.858502	0.000006	0.729158	0.11241	0.511934	0.000006	0.511327	-4.9	1884
KY-05	51.62	1.325471	0.000016	0.718041	0.12642	0.512039	0.000005	0.511356	-4.3	1839
KY-08	33.58	1.099860	0.000028	0.700121	0.29775	0.512895	0.000005	0.511268	-5.8	1966

Table 4. Zircon Hf isotopic data for the Mosuoying granites in the study area.

Analytical spot	$^{176}Yb/^{177}Hf$	1σ	$^{176}Lu/^{177}Hf$	1σ	$^{176}Hf/^{177}Hf$	1σ	$(^{176}Hf/^{177}Hf)_i$	$f_{Lu/Hf}$	εHf(t)	1σ	T_{DM1}	T_{DM2}
LREE-rich granites (KY-05)												
KY05-1	0.034185	0.000047	0.000961	0.000001	0.282190	0.000008	0.282175	-0.94	-3.2	0.3	1495	1894
KY05-2	0.034901	0.000177	0.000980	0.000006	0.282201	0.000009	0.282186	-0.93	-2.8	0.3	1481	1871
KY05-3	0.050090	0.000384	0.001402	0.000009	0.282154	0.000008	0.282132	-0.91	-4.7	0.3	1564	1989
KY05-4	0.057255	0.000841	0.001535	0.000022	0.282197	0.000007	0.282173	-0.90	-3.2	0.2	1508	1899
KY05-5	0.037510	0.000078	0.001017	0.000003	0.282210	0.000008	0.282194	-0.93	-2.5	0.3	1470	1852
KY05-6	0.038630	0.000161	0.001187	0.000010	0.282191	0.000008	0.282173	-0.92	-3.2	0.3	1503	1900
KY05-7	0.043113	0.000109	0.001200	0.000002	0.282175	0.000007	0.282156	-0.92	-3.8	0.2	1526	1936
KY05-8	0.029451	0.000178	0.000831	0.000004	0.282215	0.000007	0.282202	-0.94	-2.2	0.2	1456	1835
KY05-9	0.030116	0.000168	0.000823	0.000003	0.282210	0.000008	0.282197	-0.95	-2.4	0.3	1462	1845
KY05-10	0.028884	0.000161	0.000795	0.000003	0.282206	0.000008	0.282194	-0.95	-2.5	0.3	1467	1853
KY05-11	0.066287	0.000248	0.001850	0.000006	0.282164	0.000007	0.282135	-0.88	-4.6	0.2	1568	1982
KY05-12	0.063962	0.000166	0.001753	0.000006	0.282171	0.000007	0.282144	-0.88	-4.3	0.2	1554	1963
KY05-13	0.044720	0.000354	0.001263	0.000010	0.282185	0.000007	0.282165	-0.92	-3.5	0.2	1514	1916
KY05-14	0.041558	0.000193	0.001163	0.000004	0.282208	0.000008	0.282190	-0.92	-2.6	0.3	1478	1861
KY05-15	0.036356	0.000059	0.001027	0.000002	0.282178	0.000008	0.282162	-0.93	-3.6	0.3	1515	1923
HREE-rich granites (KY-08)												
KY08-01	0.075296	0.000243	0.002415	0.000011	0.282179	0.000009	0.282141	-0.84	-4.1	0.3	1571	1963
KY08-02	0.049670	0.000758	0.001364	0.000017	0.282219	0.000010	0.282197	-0.91	-2.2	0.4	1471	1839
KY08-04	0.048833	0.000470	0.001625	0.000011	0.282157	0.000019	0.282132	-0.89	-4.5	0.7	1568	1984
KY08-05	0.094402	0.001150	0.002758	0.000024	0.282156	0.000010	0.282113	-0.82	-5.1	0.3	1619	2026
KY08-06	0.040807	0.001470	0.001111	0.000039	0.282230	0.000011	0.282213	-0.93	-1.6	0.4	1445	1805
KY08-07	0.058103	0.002140	0.001831	0.000058	0.282209	0.000025	0.282181	-0.88	-2.7	0.9	1503	1876
KY08-10	0.095172	0.001360	0.002834	0.000062	0.282202	0.000010	0.282158	-0.81	-3.6	0.3	1555	1927
KY08-13	0.067997	0.001080	0.002134	0.000041	0.282184	0.000008	0.282150	-0.86	-3.8	0.3	1552	1943
KY08-14	0.043387	0.000744	0.001393	0.000016	0.282171	0.000012	0.282149	-0.91	-3.9	0.4	1540	1947
KY08-16	0.035592	0.000154	0.001118	0.000010	0.282200	0.000008	0.282182	-0.93	-2.7	0.3	1488	1872
KY08-17	0.038288	0.000195	0.001161	0.000006	0.282225	0.000009	0.282207	-0.92	-1.8	0.3	1455	1819
KY08-18	0.024822	0.000076	0.000750	0.000010	0.282243	0.000017	0.282231	-0.95	-1.0	0.6	1414	1764
KY08-19	0.056776	0.000676	0.001839	0.000029	0.282214	0.000010	0.282185	-0.88	-2.6	0.3	1497	1866
KY08-20	0.033511	0.000263	0.001055	0.000010	0.282249	0.000010	0.282233	-0.93	-0.9	0.4	1416	1761

Preprints.org (www.preprints.org) | NOT PEER-REVIEWED | Posted: 16 December 2024 doi:10.20944/preprints202412.1227.v1

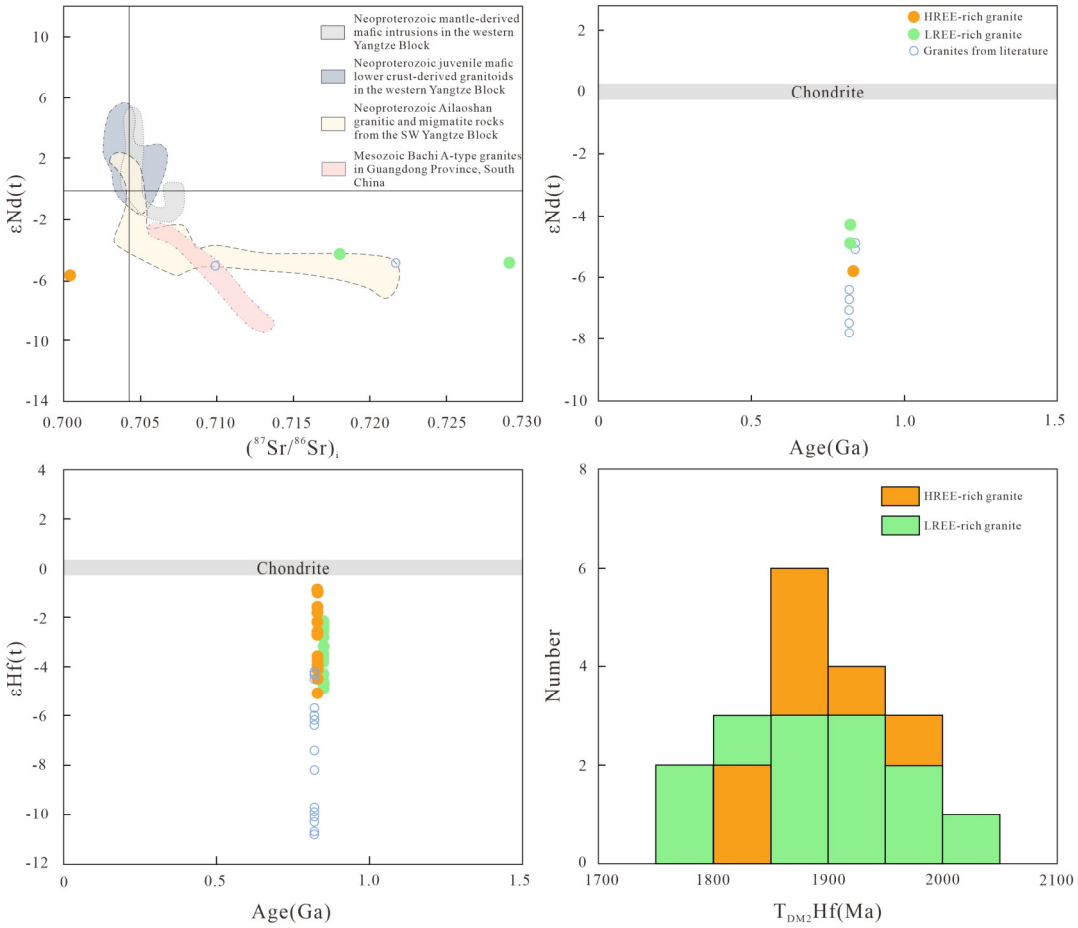

Figure 10. (a) $(^{87}Sr/^{86}Sr)_i$ vs. εNd(t) diagram (modified after [9,23]; (b) Zircon U-Pb age vs. εNd(t) diagram; (c) Zircon U-Pb age vs. εHf(t) diagram and (d) Histograms showing the εHf(t) isotope ratios and Hf model ages of the Mosuoying granites from the western margin of the Yangtze Block, South China. The data sources identical to Figure 7.

5. Discussion

5.1. REE Enrichment in the Mosuoying Granites

The contents and distribution patterns of REEs in the weathering crust are both inherited from parent rocks. Regarding the REE contents, ore-forming parent rocks with higher REE contents are more prone to form iREE deposits in their overlying weathering crust under the same conditions. Previous studies suggested that parent rocks with REE contents exceeding 150 ppm have mineralization potential [39,40]. The Mosuoying granites exhibit high total REE contents (∑REE = 266.91–553.88 ppm), serving as the prerequisite for the formation of iREE deposits in the overlying weathering crust. The REE patterns in the weathering crust depend on the ore-forming parent rocks. In other words, LREE- and HREE-rich parent rocks are prone to form LREE and HREE deposits, respectively after weathering [7,17,41]. The Mosuoying granites are primarily significantly enriched in LREEs. However, sample KY-08 display leftward REE patterns, suggesting significant HREE enrichment (Figure 9b). Hence, the study area has the potential to form iHREE deposits. The presence of various ore-forming parent rocks might be associated with multi-stage magmatic evolution.

The Mosuoying granites exhibit high silica and alkali contents, high DI (86.29–97.07), low Mg and Fe contents, low solidification index (SI: 0.50–5.45), and peraluminous characteristics (Table 2), suggesting that magmas underwent a significant crystal fractionation in their evolution. Compared to the LREE-rich granites, the HREE-rich granites exhibit higher SiO_2 contents and DI, lower Nb/Ta and Zr/Hf ratios (Figure 11a), and more prominent negative Eu anomalies, suggesting a higher degree of differentiated evolution (Figure 11). The crystal fractionation of magmas governs the enrichment and differentiation of REEs in the Mosuoying granites. Zhao et al. (2017) found that minerals formed by early magmatic crystallization are typically enriched in LREEs while HREEs are generally derived from minerals formed by late magmatic crystallization [42]. During the early stage of magmatic evolution, the fractional crystallization of LREE-rich magmatic minerals such as monazite and allanite attracted LREEs, leading to the LREE depletion and relative HREE enrichment in the residual melts [7,17,43]. During the late stage of magmatic evolution, hydrothermal

 doi:10.20944/preprints202412.1227.v1

fluids exsolved from granitic magmas were frequently enriched in volatile components, which manifested strong geochemical affinity for the migration and eventual precipitation of REEs [44]. Under certain conditions, ligand ions like F^-, CO_3^{2-}, Cl^-, and SO_4^{2-} in the volatile components would form complexes with REE^{3+} to transport REEs [15,45]. Notably, HREEs were more prone to be transported due to their smaller ionic radii, resulting in enriched HREEs in magmatic fluids [46–49]. With a decrease in the temperature of hydrothermal fluids, HREE-rich minerals such as thorite-(Y), yttrocrasite, and Y-bearing silicate gradually crystallized, providing a necessary REE source for the formation of HREE-rich granites. Additionally, the minerals formed by early magmatic crystallization might be metasomatized by hydrothermal fluids, transforming some REE-bearing minerals with strong weathering resistance into easily weathered REE-bearing minerals (Figure 13b), which provides a necessary material source for subsequent enrichment and mineralization in the weathering crust [6,47,50].

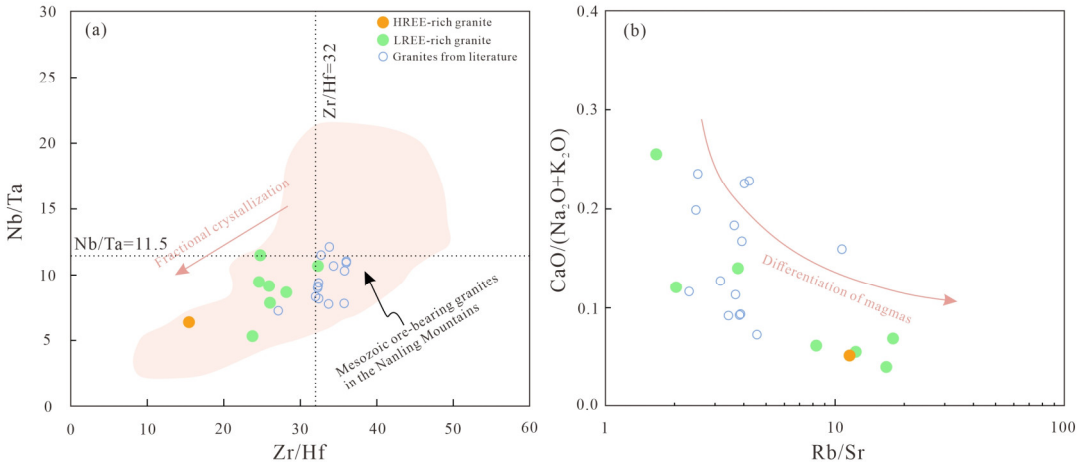

Figure 11. (a) Nb/Ta vs. Zr/Hf diagram and (b) CaO/ (Na_2O + K_2O) vs. Rb/Sr diagram (modified after [51]). Mesozoic ore-bearing granites in the Nanling Mountains referring to [42]. The data sources identical to Figure 7.

5.2. Metallogenetic Process of REE in the Parent Rock

5.2.1. Genetic Type

Given that granites are the most common ore-forming parent rocks of iREE deposits, investigating their genetic types assists in revealing the sources and metallogenetic conditions of REEs in the parent rock and further determining their mineralization processes. Granites can be categorized into A-, S-, I-, and M-types [52–54]. Since M-type granites, derived from mantle magmas, are extremely rare in the crust [55], and there is no available report on REE-rich M-type granites, this granite type is excluded from the genetic types of REE-rich granites. The other three types of ore-forming granites are widely distributed in South China, serving as the primary genetic types of the ore-forming parent rocks of iREE deposits [7]. The genetic types of granites can be determined by lithogeochemistry. Regarding the characteristics of major elements, the Mosuoying granites exhibit high SiO_2, Na_2O, and K_2O contents, high A/CNK ratios, high DI, and low CaO and MgO contents. Concerning the trace element characteristics, the Mosuoying granites are enriched in high-field-strength elements (HFSEs; e.g., Zr and Nb) and depleted in Ba, Sr, Eu, Ti, and P. These characteristics resemble those of highly fractionated aluminous A-type granites [56–60]. The (Na_2O+K_2O)/CaO *vs.* Zr+Nb+Ce+Y and Zr *vs.* 10,000Ga/Al diagrams (Figure 12a, b) show that the Mosuoying granites have high Zr+Nb+Ce+Y content (> 350 ppm) and high 10000Ga/Al ratios (> 2.6). Furthermore, all samples fall into the A-type granite zone, further corroborating that the Mosuoying granites are A-type [59,61]. In addition, temperature is identified as another crucial factor in the determination of A-type granites. The Mosuoying granites exhibit zircon saturation temperatures (T_{Zr}) exceeding 820°C (Figure 12c), indicating high-temperature magmatic sources. This is consistent with the formation temperature of A-type granites [56,58,62]. In conclusion, the Mosuoying granites are highly differentiated aluminous A-type granites.

5.2.2. Petrogenesis and REE Origin

The Mosuoying aluminous A-type granites were derived from partial melting in the crustal source, and the evidence are as follows: (1) The Mosuoying granites exhibit high SiO_2 contents, high K_2O/ Na_2O ratios, and low MgO, Cr, and Ni contents, indicating that their source is not mixed with mantle-derived materials and that the granites originated from partial melting in the crustal source [63,64]; (2) The primitive mantle-normalized trace element spidergram indicate that the granite samples are significantly enriched in Th, U, K, and Pb and depleted in Ba, Nb, Ta, Sr, and Ti. These characteristics are similar to the geochemical characteristics of the middle-upper crustal components

Preprints.org (www.preprints.org) | NOT PEER-REVIEWED | Posted: 16 December 2024 doi:10.20944/preprints202412.1227.v1

[21,65,66]; (3) The Mosuoying granites manifest negative εNd(t) values (-5.8 to -4.3) and zircon εHf(t) values (-5.1 to -0.9), which correspond to Nd-T_{2DM} and two-stage Hf model ages (Hf-T_{2DM}) ranging from 1839 to 1966 Ma and from 1761 to 2026 Ma, respectively (Figure 10). This suggests that the Mosuoying granites was derived from an ancient, mature crustal source [22,67]. In addition, given that the aluminous Mosuoying A-type granites were derived from a crustal source, possible petrogenetic mechanisms include: (1) the melting of granulite-facies metamorphosed sedimentary rocks [68]; (2) the partial melting of anhydrous lower-crustal granulitic residues [69,70]; (3) the partial melting of felsic crustal rocks (i.e., tonalities or granodiorites) in shallow parts [71–73]. Magmas from the partial melting of granulite-facies metamorphosed sedimentary rocks usually exhibit high Al_2O_3 contents and low total alkali content [53,68,74–76], which are inconsistent with those of the Mosuoying A-type granites ($Na_2O + K_2O$ = 7.03 ~ 8.34 wt.%; Al_2O_3 = 11.35 ~ 15.20 wt.%). In addition, Bonin. (2007) discovered that granulitic residues are difficult to form under high-temperature and low-pressure conditions [56]. The Mosuoying A-type granites manifest a high zircon saturation temperature (Figure 12c), indicating that the granites were formed under high-temperature condition. The $Al_2O_3/(MgO + TiO_2 + Fe_2O_3^T)$ *vs.* $Al_2O_3 + MgO + TiO_2 + Fe_2O_3$ diagram (Figure 12d) show that the granite samples largely fall into the low-pressure zone, suggesting that the Mosuoying granites were formed in a low-pressure environment (< 5 kbar). Therefore, the possibility that the Mosuoying granites originated from anhydrous lower-crustal granulitic residues can be excluded. Previous studies have revealed that the partial melting of felsic rocks (i.e., tonalities or granodiorites) from a shallow crustal source can generate A-type granites under high-temperature and low-pressure conditions [73,77]. Furthermore, the low CaO and MgO contents and significant negative Eu anomalies of A-type granites might be caused by the plagioclase-dominated residual assemblages in a low-pressure environment, and melts derived from the assemblages feature high Ga/Al ratios [73]. This characteristic corresponds to the granite samples in this study (10,000*Ga/Al = 3.27–4.21). In sum, the Mosuoying A-type granites were formed by the partial melting of shallow crustal felsic rocks under high-temperature and low-pressure conditions [22].

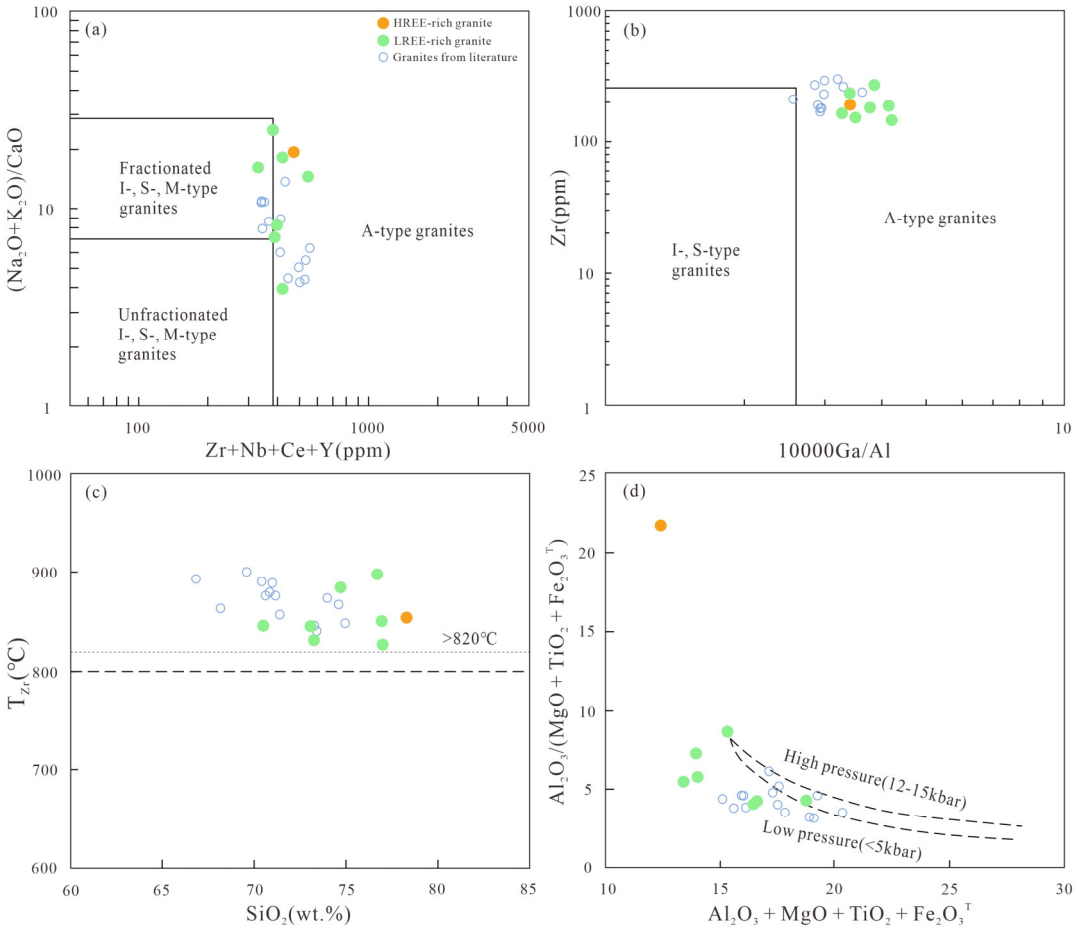

Figure 12. (a) ($Na_2O + K_2O$)/CaO vs. Zr + Nb + Ce + Y, (b) Zr vs. 10000 × Ga/Al diagram [59], (c) Zr saturation temperature (T_{Zr}) vs. SiO_2, (d) $Al_2O_3/(MgO + TiO_2 + Fe_2O_3^T)$ vs. $Al_2O_3 + MgO + TiO_2 + Fe_2O_3^T$ diagram [78]. T_{Zr} (◦C) = 12900/(ln $D^{zircon/melt}$ + 0.85 M + 2.95) − 273.5, $D^{zircon/melt}$ = 496000/Zr contents in the melts (ppm), M = molar ratio of (Na + K + 2Ca)/(Al × Si) [62]. The data sources identical to Figure 7.

 doi:10.20944/preprints202412.1227.v1

Zhu et al. (2019a) proposed that the Mosuoying granites were formed by the disequilibrium melting of the mature continental crust, with mantle-derived magmas provided only heat, rather than material sources, for the crustal melting [23]. This suggests that the high REE contents in the Mosuoying granites might be inherited from the shallow crustal felsic rocks. Under high temperatures, the partial melting of REE-rich minerals in the shallow crustal source released REEs, thereby increasing the REE contents in the melts. Additionally, the fractional crystallization of plagioclases led to increased quantities of alkaline components in the melts, further increasing the proportion of non-bridging oxygen in the residual magmas. This resulted in decreased polymerization degree and viscosity and elevated fluidity of the melts, thereby enhancing the REE retention in the melts [79]. In the late magmatic evolution, K^+ and Na^+ could increase the solubility of HREEs in the hydrothermal fluids [80]. This contributed to enhanced enrichment of HREEs in the late hydrothermal fluids and prompted the differentiation of LREEs and HREEs in the parent rock. As a result, various types of ore-forming granites were formed.

5.2.3. Formation Process of REE-Rich Granites

The formation of A-type granites tends to be associated with an extensional tectonic setting during late subduction [59,81]. Zhang. (2024) corroborated that the Mosuoying granites are A_2-type granites, suggesting they were formed in a post-collisional or back-arc extensional setting [22]. Their shallow crustal source further indicate that the Mosuoying granitic pluton was derived from a non-compressional tectonic setting [67]. Based on these conclusions, we proposed a hypothesis about the formation process of the REE-rich Mosuoying granite. Specifically, during the continuous eastward subduction of the oceanic slab beneath the western margin of the Neoproterozoic Yangtze Block, the oceanic slab underwent break-off due to gravitational sinking, probably leading to large-scale slab melting and the gradual formation of slab window. The mantle asthenosphere-derived materials would experience upwelling along the slab window and heat the overlying lithospheric mantle and middle-lower crust [22]. In the non-compressional tectonic setting, the crust tended to thin, allowing the high-temperature heat source to sufficiently reach the shallow crust. This induced the partial melting of the REE-rich felsic rocks to release REEs (Figure 13a). Such a transcrustal magmatic system would induce the migration of magma chambers and result in intense magmatic differentiation. Consequently, evolved melts and volatiles-rich hydrothermal fluids were formed, creating necessary conditions for the enrichment and differentiation of REEs in subsequent magmatic-hydrothermal evolution processes [82,83]. Concurrently, high-temperature A-type granitic magmas enhanced the solubility of REEs in the melts, thus inhibiting the separation of REE-rich minerals from the melts [9]. This might be an important factor in the enrichment of REEs in the Mosuoying A-type granites. When the REE-rich melts intruded into a certain depth, their temperature and pressure decreased continuously, and LREE-rich minerals such as monazite and titanite would be preferentially separated from the melts to form LREE-rich granites. The fractional crystallization of LREE-rich minerals led to the enrichment of HREEs in the residual magmas. In the late stage of magmatic evolution, the hydrothermal fluids derived from the granitic magmas were rich in volatile components, where the ligand ions would form complexes with REE^{3+} (especially $HREE^{3+}$) to migrate REEs. As a result, a series of HREE-rich hydrothermal minerals were formed, providing a necessary material source for the formation of HREE-rich granites (Figure 13b).

Preprints.org (www.preprints.org) | NOT PEER-REVIEWED | Posted: 16 December 2024 doi:10.20944/preprints202412.1227.v1

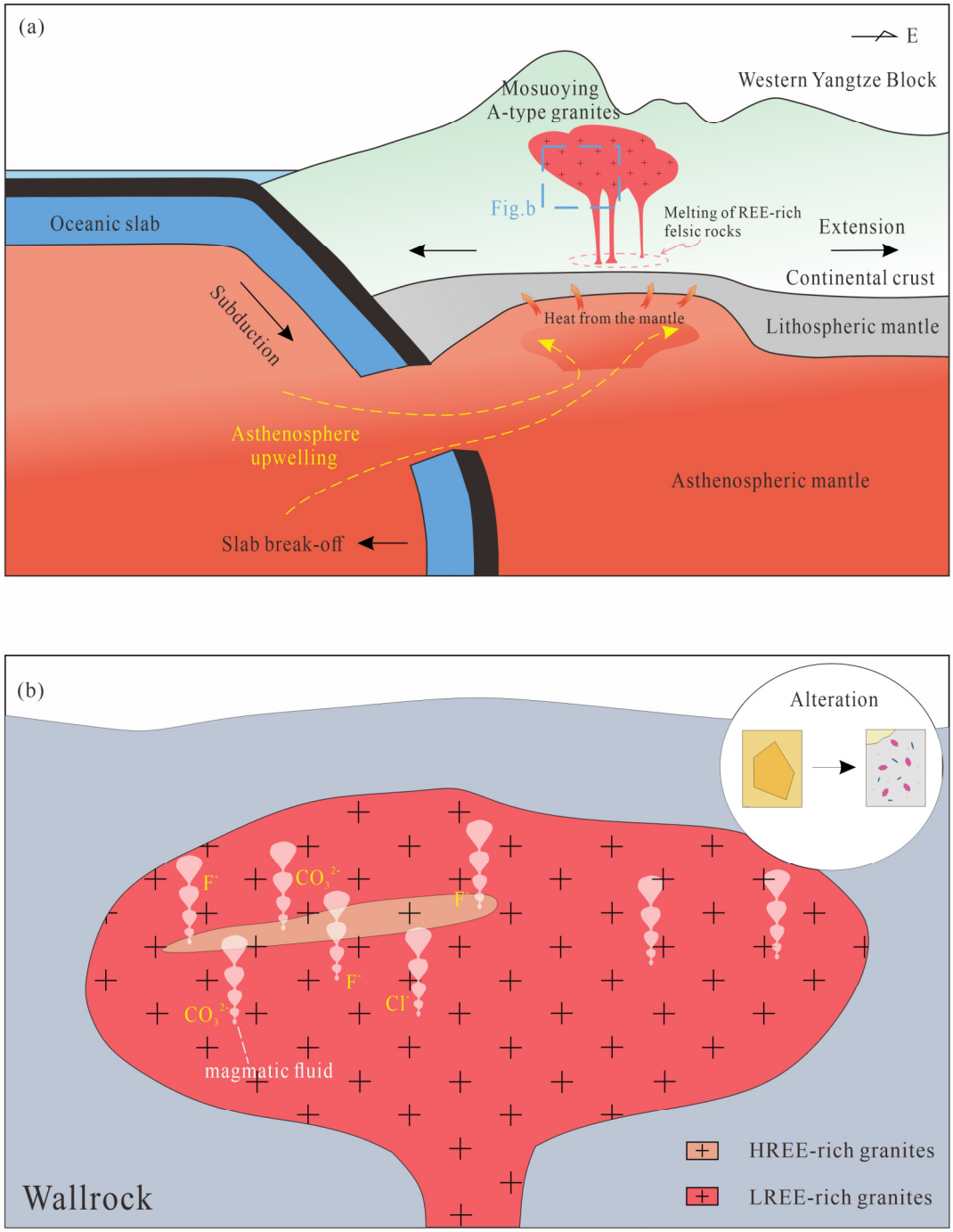

Figure 13. Conceptual model for the generation of Neoproterozoic REE-rich Mosuoying granite in the Dechang area. Figure 13b modified after [84].

6. Conclusions

(1) The Mosuoying granites exhibit LREE enrichment primarily and significant HREE enrichment in some ore blocks. The occurrence of different types of ore-forming parent rocks might be related to the magmatic crystal fractionation and the hydrothermal fluids exsolved from granitic magmas during the evolution of magmatic and hydrothermal systems.

(2) The Mosuoying granites are identified as highly differentiated alumina A-type granites, and their high REE contents might originate from the partial melting of shallow crustal felsic rocks under high-temperature and low-pressure conditions. In the back-arc extensional setting along the western margin of the Neoproterozoic Yangtze Block, high-temperature mantle asthenosphere-derived magmas experienced upwelling along slab window and heated the overlying crust. The non-compressional tectonic settings led to crustal thinning, allowing the high-temperature heat

 doi:10.20944/preprints202412.1227.v1

source to reach the shallow crust. This induced the partial melting of the felsic rocks to release REEs, and REE-rich Mosuoying granites were formed during multi-stage magmatic evolution.

Author Contributions: Writing—original draft preparation, X.X.; writing—review and editing, G.L. and L.Q.; methodology, S.D.; resources, L.O.; funding acquisition, G.L. All authors have read and agreed to the published version of the manuscript.

Funding: This research was funded by the Scientific Research Fund for the Doctoral Program of Xichang University (YBZ202263).

Data Availability Statement: Data are contained within the article.

Acknowledgments: Analytical data provided by Langfang Shangyi Geological Exploration Technical Services Co., Ltd and Institute of Mineral Comprehensive Utilization of CAGS, thanks to the units and individuals for the help of this article.

Conflicts of Interest: There is no conflicts of interest relevant to this article. Author Xuepeng Xiao has received research grants from Xichang University. The funding sponsors had no role in the design of the study; in the collection, analyses, or interpretation of data; in the writing of the manuscript, or in the decision to publish the results.

References

1. Balaram, V. Rare earth elements: A review of applications, occurrence, exploration, analysis, recycling, and environmental impact. *Geoscience Frontiers* **2019**, *10*, 1285-1303.
2. Fan, H.; Hecai, N.; Xiaochun, L.; Kuifeng, Y.; Zhanfeng, Y.; Qiwei, W. The types, ore genesis and resource perspective of endogenic ree deposits in china. *Chinese Science Bulletin* **2020**, *65*, 3778-3793.
3. Charalampides, G.; Vatalis, K.I.; Apostoplos, B.; Ploutarch-Nikolas, B. Rare earth elements: Industrial applications and economic dependency of europe. *Procedia Economics and Finance* **2015**, *24*, 126-135.
4. Simandl, G.J. Geology and market-dependent significance of rare earth element resources. *Mineralium Deposita* **2014**, *49*, 889-904.
5. Kynicky, J.; Smith, M.P.; Xu, C. Diversity of rare earth deposits: The key example of china. *Elements* **2012**, *8*, 361-367.
6. Bao, Z.; Zhao, Z. Geochemistry of mineralization with exchangeable rey in the weathering crusts of granitic rocks in south china. *Ore Geology Reviews* **2008**, *33*, 519-535.
7. Li, Y.H.M.; Zhao, W.W.; Zhou, M.F. Nature of parent rocks, mineralization styles and ore genesis of regolith-hosted ree deposits in south china: An integrated genetic model. *Journal of Asian Earth Sciences* **2017**, *148*, 65-95.
8. Yang, Y.Y.; Li, N.B.; Jiang, Y.H.; Zhao, X. Geochemical differences of parent rocks for ion-adsorption lree and hree deposits: A case study of the guanxi and dabu granite plutons. *Geotectonica et Metallogenia* **2024**, *48*, 232-247.
9. Zhao, X.; Li, N.B.; Huizenga, J.M.; Yan, S.; Yang, Y.Y.; Niu, H.C. Rare earth element enrichment in the ion-adsorption deposits associated granites at mesozoic extensional tectonic setting in south china. *Ore Geology Reviews* **2021**, *137*, 104317.
10. Zhao, X.; Li, N.B.; Marten Huizenga, J.; Zhang, Q.B.; Yang, Y.Y.; Yan, S.; Yang, W.b.; Niu, H.C. Granitic magma evolution to magmatic-hydrothermal processes vital to the generation of hrees ion-adsorption deposits: Constraints from zircon texture, u-pb geochronology, and geochemistry. *Ore Geology Reviews* **2022a**, *146*, 104931.
11. Sanematsu, K.; Watanabe, Y. Characteristics and genesis of ion adsorption-type rare earth element deposits. In *Rare Earth and Critical Elements in Ore Deposits*, Society of Economic Geologists: Rev. Econ. Geol, 2016; Vol. 18, pp 55-79.
12. Zhao, X.; Li, N.B.; Niu, H.C.; Jiang, Y.H.; Yan, S.; Yang, Y.Y.; Fu, R.X. Hydrothermal alteration of allanite promotes the generation of ion-adsorption lree deposits in south china. *Ore Geology Reviews* **2023**, *155*, 105377.
13. Zhao, X.; Li, N.B.; Niu, H.C.; Wang, J.; Yan, S.; Yang, Y.Y.; Fu, R.X.; Huizenga, J.M. Hree enrichment during magmatic evolution recorded by apatite: Implication for the ion-adsorption hree mineralization in south china. *Lithos* **2022b**, *432-433*, 106896.
14. Fan, C.; Xu, C.; Shi, A.; Smith, M.P.; Kynicky, J.; Wei, C. Origin of heavy rare earth elements in highly fractionated peraluminous granites. *Geochimica et Cosmochimica Acta* **2023**, *343*, 371-383.
15. Xu, C.; Kynický, J.; Smith, M.P.; Kopriva, A.; Brtnický, M.; Urubek, T.; Yang, Y.; Zhao, Z.; He, C.; Song, W. Origin of heavy rare earth mineralization in south china. *Nature Communications* **2017**, *8*, 14598.
16. Dou, J.Z.; Wang, Y.; Tan, W.; Song, Z.Z. Mechanism of ree enrichment in granitic bedrocks of the ion-adsorption ree deposits in the nanling mountain range, south china. *Geotectonica et Metallogenia* **2024**, *48*, 200-212.
17. Zhao, Z.; Wang, D.; Bagas, L.; Chen, Z. Geochemical and ree mineralogical characteristics of the zhaibei granite in jiangxi province, southern china, and a model for the genesis of ion-adsorption ree deposits. *Ore Geology Reviews* **2022**, *140*, 104579.
18. Xia, X.H.; Liu, T.Q.; Yin, C.; Yang, W.; Tan, H.Q.; Zhou, J.Y.; Wang, C.H. First discovery of ion adsorption-type (medium—heavy) ree depositin the panzhihua—xichang area, sichuan province, and its significance. *Geological Review* **2022**, *68*, 1540-1543.
19. Zou, J.Z.; Fei, N.; Guo, J.C. New discovery of ion-absorption type ree mineral occurrence in the mianning-dechang area, sichuan province. *Geology in China* **2023**, *50*, 648-649.
20. Xia, X.H.; Liu, T.Q.; Yin, C.; Duan, L.; Yang, W.; Wang, C.; Li, N.; Wang, C.H.; Tan, H.Q. Geological characteristics and metallogenic factors of the kuanyu ion adsorption-type ree deposit in the panzhihua-xichang district, sichuan, sw china and its prospecting potential. *Geology in China* **2023**, 1-18.
21. Guo, C.L.; Wang, D.H.; Chen, Y.C.; Zhao, Z.G.; Wang, Y.B.; Fu, X.F.; Fu, D.M. Shrimp u-pb zircon ages and major element, trace element and nd-sr isotope geochemical studies of a neoproterozoic granitic complex in western sichuan: Petrogenesis and tectonic significance. *Acta Petrologica Sinica* **2007**, 2457-2470.

22. Zhang, J.B.; Shi, C.L.; Liu, P.W.; Liu, Y.X.; Ding, X.Z.; Zhang, H.; Yang, Y.M.; Qian, B. Neoproterozoic slab window in the western yangtze block, south china: Evidence from adakitic granodiorites, gabbro-diorites and high-k granites in the panxi arc belt. *Journal of Asian Earth Sciences* **2024**, *259*, 105859.
23. Zhu, Y.; Lai, S.C.; Qin, J.F.; Zhu, R.Z.; Zhang, F.Y.; Zhang, Z.Z.; Zhao, S.W. Neoproterozoic peraluminous granites in the western margin of the yangtze block, south china: Implications for the reworking of mature continental crust. *Precambrian Research* **2019a**, *333*, 105443.
24. Huang, J.Q.; Ren, J.S.; Jiang, C.F.; Zhang, Z.M.; Xu, Z.Q. An outline of the tectonic characteristics of china. *Acta Geologica Sinica* **1977**, 117-135.
25. Hou, Z.; Tian, S.; Xie, Y.; Yang, Z.; Yuan, Z.; Yin, S.; Yi, L.; Fei, H.; Zou, T.; Bai, G., *et al.* The himalayan mianning–dechang ree belt associated with carbonatite–alkaline complexes, eastern indo-asian collision zone, sw china. *Ore Geology Reviews* **2009**, *36*, 65-89.
26. Gan, L.; Yan, B.; Liu, Y.; Gao, Y.; Yin, C.; Zhu, L.; Tan, S.; Ding, D.; Jiang, H. Geochemical and mineralogical characteristics of ion-adsorption type ree mineralization in the mosuoying granite, panxi area, southwest china. *Minerals* **2023**, *13*, 1449.
27. Mabi, A.W.; Yang, Z.X.; Zhang, M.C.; Wen, D.K.; Li, Y.L.; Liu, X.Y. Two types of granites in the western yangtze block and their implications for regional tectonic evolution: Constraints from geochemistry and isotopic data. *Acta Geologica Sinica(English Edition)* **2018**, *92*, 89-105.
28. Sláma, J.; Košler, J.; Condon, D.J.; Crowley, J.L.; Gerdes, A.; Hanchar, J.M.; Horstwood, M.S.A.; Morris, G.A.; Nasdala, L.; Norberg, N., *et al.* Plešovice zircon — a new natural reference material for u–pb and hf isotopic microanalysis. *Chemical Geology* **2008**, *249*, 1-35.
29. Ludwig, K.R. Isoplot 3.00: A geochronological toolkit for microsoft excel: Berkeley geochronology center. *Special Publication* **2003**, *No. 4*.
30. Hoskin, P.W.O.; Schaltegger, U. The composition of zircon and igneous and metamorphic petrogenesis. *Reviews in Mineralogy and Geochemistry* **2003**, *53*, 27-62.
31. Hu, C.X.; Yuan, W.M. Zircon characteristics of different genetic types and their geochronological significance. *China Mining Magazine* **2021**, *30*, 204-207.
32. Rubatto, D.; Gebauer, D. Use of cathodoluminescence for u-pb zircon dating by ion microprobe: Some examples from the western alps. *Cathodoluminescence in Geosciences* **2000**, 373-400.
33. Wetherill, G.W. Discordant uranium-lead ages, i *Transactions, American Geophysical Union* **1956**, *Vol.37*, 320-326.
34. Middlemost, E.A.K. Naming materials in the magma/igneous rock system. *Earth-Science Reviews* **1994**, *37*, 215-224.
35. Peccerillo, A.; Taylor, S.R. Geochemistry of eocene calc-alkaline volcanic rocks from the kastamonu area, northern turkey. *Contributions to Mineralogy and Petrology* **1976**, *58*, 63-81.
36. Maniar, P.D.; Piccoli, P.M. Tectonic discrimination of granitoids. *GSA Bulletin* **1989**, *101*, 635-643.
37. Wright, J.B. A simple alkalinity ratio and its application to questions of non-orogenic granite genesis. *Geological Magazine* **1969**, *106*, 370-384.
38. Sun; Publications, M.J.G.S.L.S. Chemical and isotopic systematics of oceanic basalts: Implications for mantle composition and processes. *Geol. Soc., London, Spec. Publ.* **1989**, *42*.
39. Bai, G.; Wu, C.Y.; Ding, X.S.; Yuan, Z.X.; Huang, D.H.; Huang, P.H. *Genesis and spatial distribution of ion-adsorption type ree deposit in nanling region*. Institute of Ore Deposit Geology, Beijing, p, 1989; Vol. 105.
40. Lu, L.; Wang, D.H.; Wang, C.H.; Zhao, Z.; Feng, W.J.; Xu, X.C.; Chen, C.; Zhong, H.R. The metallogenic regularity of ion-adsorption type ree deposit in yunnan province. *Acta Geologica Sinica* **2020**, *94*, 179-191.
41. Pan, Z.W.; Lu, Y.X.; Luo, J.H.; Tang, Z.; Yu, H.J.; Su, X.Y.; Yang, Q.B.; Fu, H. Ree distribution characteristics of the yingpanshan ion adsorption type rare-earth deposit in the longchuan area of western yunnan. *Geology and Exploration* **2021**, *57*, 784-795.
42. Zhao, Z.; Wang, D.H.; Chen, Z.H.; Chen, Z.Y. Progress of research on metallogenic regularity of ion-adsorption type ree deposit in the nanling range. *Acta Geologica Sinica* **2017**, *91*, 2814-2827.
43. Yang, X.M. Using rare earth elements (ree) to decipher the origin of ore fluids associated with granite intrusions *Minerals* **2019**, *9*, 426.
44. Candela, P.A. A review of shallow, ore-related granites: Textures, volatiles, and ore metals. *Journal of Petrology* **1997**, *38*, 1619-1633.
45. Migdisov, A.A.; Williams-Jones, A.E.; Wagner, T. An experimental study of the solubility and speciation of the rare earth elements (iii) in fluoride- and chloride-bearing aqueous solutions at temperatures up to 300°c. *Geochimica et Cosmochimica Acta* **2009**, *73*, 7087-7109.
46. Choppin, G.R. In *Factors in the complexation of lanthanides. In: Lundin c e, ed*, Proc of the Rare Earth Res Conf, 12th, Vail, CO, USA, 1976; Vail, CO, USA, pp 130-139.
47. Huang, D.H., Wu, Cheng Y, Han, JiuZhu Ree geochemistry and mineralization characteristics of the zudong and gnanxi granites, jiangxi province. *Acta Geologica Sinica(English Edition)* **1989**, 139-157.
48. Rolland, Y.; Cox, S.; Boullier, A.M.; Pennacchioni, G.; Mancktelow, N. Rare earth and trace element mobility in mid-crustal shear zones: Insights from the mont blanc massif (western alps). *Earth and Planetary Science Letters* **2003**, *214*, 203-219.
49. Wood, S.A. The aqueous geochemistry of the rare-earth elements and yttrium: 1. Review of available low-temperature data for inorganic complexes and the inorganic ree speciation of natural waters. *Chemical Geology* **1990**, *82*, 159-186.
50. Bern, C.R.; Yesavage, T.; Foley, N.K. Ion-adsorption rees in regolith of the liberty hill pluton, south carolina, USA: An effect of hydrothermal alteration. *Journal of Geochemical Exploration* **2017**, *172*, 29-40.

51. Qin, Z.W.; Fu, J.M.; Xing, G.F.; Cheng, S.B.; Lu, Y.Y.; Zhu, Y.X. The petrogenetic differences of the middle-late jurassic w-, sn-, pb-zncu-bearing granites in the nanling range, south china. *Geology in China* **2022**, *49*, 518-541.
52. Chappell, B.W.; White, A.J.R. Two constrasting granite types. *Pacific Geology* **1974**, *8*, 173-174.
53. Chappell, B.W.; White, A.J.R. I- and s-type granites in the lachlan fold belt. *Trans. R. Soc. Edinb. Earth Sci.* **1992**, *79*, 169-181.
54. Wu, F.Y.; Li, X.H.; Yang, J.H.; Zheng, Y.H. Discussions on the petrogenesis of granites. *Acta Petrologica Sinica* **2007**, 1217-1238.
55. Whalen, J.B. Geochemistry of an island-arc plutonic suite: The uasilau-yau yau intrusive complex, new britain, p.N.G. *Journal of Petrology* **1985**, *26*, 603-632.
56. Bonin, B. A-type granites and related rocks: Evolution of a concept, problems and prospects. *Lithos* **2007**, *97*, 1-29.
57. Eby, G.N. The a-type granitoids: A review of their occurrence and chemical characteristics and speculations on their petrogenesis. *Lithos* **1990**, *26*, 115-134.
58. King, P.L.; White, A.J.R.; Chappell, B.W.; Allen, C.M. Characterization and origin of aluminous a-type granites from the lachlan fold belt, southeastern australia. *Journal of Petrology* **1997**, *38*, 371-391.
59. Whalen, J.B.; Currie, K.L.; Chappell, B.W. A-type granites: Geochemical characteristics, discrimination and petrogenesis. *Contributions to Mineralogy and Petrology* **1987**, *95*, 407-419.
60. Wu, F.; Liu, X.; Ji, W.; Wang, J.M.; Yang, L. Highly fractionated granites: Recognition and research. *Science China Earth Sciences* **2017**, *60*, 1201-1219.
61. Li, X.W.; Mo, X.X.; Zhao, Z.D.; Zhu, D.C. A discussion on how to discriminate a-type granite. *Geological Bulletin of China* **2010**, *29*, 278-285.
62. Watson, E.B.; Harrison, T.M. Zircon saturation revisited: Temperature and composition effects in a variety of crustal magma types. *Earth and Planetary Science Letters* **1983**, *64*, 295-304.
63. Du, L.; Long, X.; Yuan, C.; Zhang, Y.; Huang, Z.; Sun, M.; Xiao, W. Petrogenesis of late paleozoic diorites and a-type granites in the central eastern tianshan, nw china: Response to post-collisional extension triggered by slab breakoff. *Lithos* **2018**, *318-319*, 47-59.
64. Karsli, O.; Aydin, F.; Uysal, I.; Dokuz, A.; Kumral, M.; Kandemir, R.; Budakoglu, M.; Ketenci, M. Latest cretaceous “a2-type” granites in the sakarya zone, ne turkey: Partial melting of mafic lower crust in response to roll-back of neo-tethyan oceanic lithosphere. *Lithos* **2018**, *302-303*, 312-328.
65. Pearce, J.A.; Peate, D.W. Tectonic implications of the composition of volcanic arc magmas. *Annual Review of Earth and Planetary Sciences* **1995**, *23*, 251-285.
66. Rudnick, R.; Gao, S. The role of lower crustal recycling in continent formation. *Geochimica et Cosmochimica Acta* **2003**, *67*, A403.
67. Zhu, Y.; Lai, S.C.; Qin, J.F.; Zhu, R.Z.; Zhang, F.Y.; Zhang, Z.Z.; Gan, B.P. Petrogenesis and geodynamic implications of neoproterozoic gabbro-diorites, adakitic granites, and a-type granites in the southwestern margin of the yangtze block, south china. *Journal of Asian Earth Sciences* **2019b**, *183*, 103977.
68. Huang, H.Q.; Li, X.H.; Li, W.X.; Li, Z.X. Formation of high δ^{18}o fayalite-bearing a-type granite by hightemperature melting of granulitic metasedimentary rocks, southern china. *Geology* **2011**, *39*, 903-906.
69. Clemens, J.D.; Holloway, J.R.; White, A.J.R. Origin of an a-type granite; experimental constraints. *American Mineralogist* **1986**, *71*, 317-324.
70. Collins, W.J.; Beams, S.D.; White, A.J.R.; Chappell, B.W. Nature and origin of a-type granites with particular reference to southeastern australia. *Contributions to Mineralogy and Petrology* **1982**, *80*, 189-200.
71. Chen, J.; Fu, L.; Wei, J.; Selby, D.; Zhang, D.; Zhou, H.; Zhao, X.; Liu, Y. Proto-tethys magmatic evolution along northern gondwana: Insights from late silurian–middle devonian a-type magmatism, east kunlun orogen, northern tibetan plateau, china. *Lithos* **2020**, *356-357*, 105304.
72. Frost, C.D.; Frost, B.R. On ferroan (a-type) granitoids: Their compositional variability and modes of origin. *Journal of Petrology* **2011**, *52*, 39-53.
73. Patiño Douce, A.E. Generation of metaluminous a-type granites by low-pressure melting of calc-alkaline granitoids. *Geology* **1997**, *25*, 743-746.
74. Creaser, R.A.; Price, R.C.; Wormald, R.J. A-type granites revisited. Assessment of a residual-source model. *Geology* **1991**, *19*, 163-163.
75. Deng, X.; Zhao, T.; Peng, T. Age and geochemistry of the early mesoproterozoic a-type granites in the southern margin of the north china craton: Constraints on their petrogenesis and tectonic implications. *Precambrian Research* **2016**, *283*, 68-88.
76. Sylvester, P.J. Post-collisional strongly peraluminous granites. *Lithos* **1998**, *45*, 29-44.
77. Breiter, K. Nearly contemporaneous evolution of the a- and s-type fractionated granites in the krušné hory/erzgebirge mts., central europe. *Lithos* **2012**, *151*, 105-121.
78. Patiño Douce, A.E. What do experiments tell us about the relative contributions of crust and mantle to the origin of granitic magmas? . *Geological Society, London, Special Publications* **1999**, *168*, 55-75.
79. Tao, X.Y. The differentiation mechanism of rare earth elements in parent rocks of ion adsorption-type rare earth element deposits D, China University of Geosciences Beijing, 2020.
80. Anenburg, M.; Mavrogenes, J.A.; Frigo, C.; Wall, F. Rare earth element mobility in and around carbonatites controlled by sodium, potassium, and silica. *Science Advances* **2020**, *6*, 1-10.
81. Eby, G.N. Chemical subdivision of the a-type granitoids: Petrogenetic and tectonic implications. *Geology* **1992**, *20*, 641-644.
82. Cao, M.X.; Wang, X.G.; Zhang, D.F.; Zhang, Y.W.; Gong, L.X.; Zhong, W. Petrogenesis and ree mineralogical characteristics of shitouping granites in southern jiangxi province: Implication for hree mineralization in south china. *Ore Geology Reviews* **2024**, *168*, 106011.

 doi:10.20944/preprints202412.1227.v1

83. Xu, X.S.; Zhao, K.; He, Z.Y.; Liu, L.; Hong, W.T. Cretaceous volcanic-plutonic magmatism in se china and a genetic model. *Lithos* **2021**, *402-403*, 105728.
84. Chu, G.; Chen, H.; Feng, Y.; Wu, C.; Li, S.; Zhang, Y.; Lai, C.-K. Are south china granites special in forming ion-adsorption ree deposits? *Gondwana Research* **2024**, *125*, 82-90.